Energy Optimal Path Planning Using Stochastic Dynamically Orthogonal Level Set Equations

ARCHIVES
MASSACHUSETTS INSTITUTE
OF TECHNOLOGY
OCT 09 2014
LIBRARIES

by

Deepak Narayanan Subramani

B.Tech and M.Tech, Indian Institute of Technology Madras, India

Submitted to the School of Engineering
in partial fulfillment of the requirements for the degree of

Master of Science in Computation for Design and Optimization

at the

MASSACHUSETTS INSTITUTE OF TECHNOLOGY

September 2014

© Massachusetts Institute of Technology 2014. All rights reserved.

Signature redacted

Author ....
School of Engineering
August 20, 2014

Signature redacted

Certified by ....
Pierre F.J Lermusiaux
Associate Professor, Department of Mechanical Engineering
Thesis Supervisor

Signature redacted

Accepted by ....
Nicolas Hadjiconstantinou
Co-Director, Computation for Design and Optimization

Energy Optimal Path Planning Using Stochastic Dynamically Orthogonal Level Set Equations

by

Deepak Narayanan Subramani

Submitted to the School of Engineering
on August 20, 2014, in partial fulfillment of the
requirements for the degree of
Master of Science in Computation for Design and Optimization

Abstract

The growing use of autonomous underwater vehicles and underwater gliders for a variety of applications gives rise to new requirements in the operation of these vehicles. One such important requirement is optimization of energy required for undertaking missions that will enable longer endurance and lower operational costs. Our goal in this thesis is to develop a computationally efficient, and rigorous methodology that can predict energy-optimal paths from among all time-optimal paths to complete an underwater mission. For this, we develop rigorous a new stochastic Dynamically Orthogonal Level Set optimization methodology.

In our thesis, after a review of existing path planning methodologies with a focus on energy optimality, we present the background of time-optimal path planning using the level set method. We then lay out the questions that inspired the present thesis, provide the goal of the current work and explain an extension of the time-optimal path planning methodology to the time-optimal path planning in the case of variable nominal engine thrust. We then proceed to state the problem statement formally. Thereafter, we develop the new methodology for solving the optimization problem through stochastic optimization and derive new Dynamically Orthogonal Level Set Field equations. We then carefully present different approaches to handle the non-polynomial non-linearity in the stochastic Level Set Hamilton-Jacobi equations and also discuss the computational efficiency of the algorithm. We then illustrate the inner-workings and nuances of our new stochastic DO level set energy optimal path planning algorithm through two simple, yet important, canonical steady flows that simulate a stead front and a steady eddy. We formulate a double energy-time minimization to obtain a semi-analytical energy optimal path for the steady front crossing test case and compare the results to these of our stochastic DO level set scheme. We then apply our methodology to an idealized ocean simulation using Double Gyre flows, and finally show an application with real ocean data for completing a mission in the Middle Atlantic Bight and New Jersey Shelf/Hudson Canyon region.

Thesis Supervisor: Pierre F.J Lermusiaux
Title: Associate Professor, Department of Mechanical Engineering

Acknowledgments

I sincerely thank my advisor, Prof Pierre Lermusiaux, for for his words of encouragement, timely help, and guidance. I specially thank him for carefully reviewing the present thesis. I thank Pat for helping me with real ocean application presented in the thesis, and also for all the general help especially with coding. I thank Tapovan for insightful discussions and for patiently answering all my questions throughout this work. With the MSEAS group, we are grateful to the Office of Naval Research for research support under grants N00014-09-1-0676 (Science of Autonomy - A-MISSION) and N00014-14-1-0476 (Science of Autonomy - LEARNS) to the Massachusetts Institute of Technology. My education at MIT would not have been possible without these generous grants. We also thank all of our colleagues involved in collecting observations during SW06 and AWACS-06 that allowed the realistic simulations component of the present study.

Life at MIT is fun because of all the people here. I thank Jen, Jing, Chris, Akash, Wayne, Sydney, John, and Marcia for friendship and help during the course of my work at MSEAS group. Special thanks to Barbara and Kate at the CDO office.

My gratitude to Prof Balaji, whose words inspire and drive me forward cannot be repeated enough. Many thanks to Srinivasa Ramanujam whose advice I cherish in moments of doubt. Thanks to Jaichander for long academic, spiritual and general conversations. I thank my parents and sister for all their support and help, especially in the last month leading to the preparation of this thesis. I also take this opportunity to thank all those people whom I have met both at IIT and MIT whose lives serve as motivation for making a positive impact to the world.

Contents

1 Introduction **17**

2 Literature Review **21**

3 Background and Problem Statement **27**

3.1 Time-Optimal Path Planning using Level Set Methods 27

3.2 New Questions 28

3.3 Goal 29

3.4 Time-Optimal Path Planning using the level-set Hamilton Jacobi equation: provided time dependent engine speed 30

3.5 Problem Statement 31

3.6 Conclusion 32

4 Methodology **35**

4.1 Introduction 35

4.2 Stochastic Optimization Setup 37

4.3 Dynamically Orthogonal Equations 38

4.4 Stochastic Simulation 39

4.4.1 DO-MC Gamma 41

4.4.2 DO-KL Gamma 41

4.4.3 Comments/Remarks 43

4.5 Optimization 44

4.6 Brief Derivations 45

4.6.1 DO-MC Gamma Derivation 45

4.6.2 DO-KL Gamma Derivation 46

4.6.3 DO-Taylor Gamma Derivation 48

4.7 Conclusion 49

5 Algorithm **51**

5.1 Overall Algorithm 51

5.2 $F(t;\omega)$ sampling 51

5.3 Numerical Stochastic DO-Level Set Simulation 52

5.3.1 Initial and boundary condition for DO equations 52

5.3.2 Numerics 53

5.3.3 Various tests 53

5.4 Optimization 53

5.5 Conclusion 53

6 Applications: Canonical Steady Flows **57**

6.1 Introduction 57

6.2 Jet flow: Simulated Steady Front 57

6.2.1 Benchmark Solution 58

6.2.2 Illustration of the algorithm 63

6.3 Steady Circular Flow 69

6.3.1 Energy optimal Path Planning 69

6.4 Validation of stochastic DO-level set optimization 71

6.4.1 Comparison of DO-MC Gamma, DO-KL Gamma, and DO-Taylor Gamma with Monte Carlo 71

6.5 Conclusion 72

7 Applications: Idealized and Realistic Ocean Simulation **79**

7.1 Introduction 79

7.2 Idealized Ocean Simulation 79

7.2.1 Double Gyre 80

7.2.2 Energy Path Planning in a Double Gyre Flow Field 85
7.3 Realistic Data-driven Ocean Simulation 85
7.3.1 Data-assimilative primitive-equation ocean simulations 85
7.3.2 Energy Optimal Path Planning for Mission 87
7.4 Conclusion 88

8 Conclusion and Future Work **91**

List of Figures

1-1 General definition of path planning is the task of designing a path for mobile robot to navigate from start point (s) to a desired goal (f) by optimizing a set of objective criterion 18

1-2 (a) is a Slocum glider (b) is SeaExplorer, a propelled AUV from ACSA ALCEN. (Wikipedia, 2012) 18

3-1 Goal of the present work is to compute the energy optimal path(s) among all the time optimal paths from point A to point B (Lolla et al., 2012). 30

5-1 Flowchart depicting different steps of the algorithm 54

5-2 Samples of $F(t;\omega)$ from different sampling strategies 55

5-3 List of various tests performed 56

6-1 The domain with a simulated steady front used for testing and illustrating the algorithm developed in this thesis 58

6-2 Parameters involved in optimal crossing of a jet flow: jet speed V and width d; start (circle), end (star), distances, vehicle nominal speed and headings are marked. Adapted from Lolla (2012) 58

6-3 $F_{\mathrm{DO}}(t;r)$ samples using different strategies. In the first row, we show all 10,000 samples of $F_{\mathrm{DO}}(t;r)$ used for optimal Steady Front Crossing Path Planning. In the second row, we show representative $F_{\mathrm{DO}}(t;r)$ samples for clarity. 64

6-4 Figure shows the evolution of zero level set contours for vehicles (samples) with slowest ($F_{\min}$), fastest ($F_{\max}$), and an intermediate nominal engine speeds. We see that the slowest vehicle travelling at 5cm/s is not able to cross the steady front within 150 hrs. Zero level set of all samples will be located spatially within the zero level sets of slowest and fastest samples. 65
6-5 Figure shows Energy Cost Function vs Time using different power functions of nominal engine speed $F(t)$. 66
6-6 Figure shows Energy Cost Function vs Time for 30,000 (10,000×3) samples. The figure shows the optimal energy envelop obtained by each sampling strategy. We note that vehicles (samples) which vary the engine speed on their steady front crossing mission have energy requirements lower than those vehicles which use single engine speed for the mission. The algorithm is able to identify such nominal engine speed design which results in optimal energy for the mission paths in the class of F(t) sampling. 67
6-7 For a time to reach of $t = 104.6$ we show the optimal engine speed obtained in the three classes of sampling 68
6-8 For a time to reach of $t = 104.6$ we show the optimal paths compared to the path which uses constant speed 68
6-9 The flow field for steady circular flow 69
6-10 Using three stochastic DO level-set simulations for exploring energy utilization by vehicles in a circular flow 70
6-11 Paths for circular flow 70
6-12 Comparing the level set evolution by the stochastic DO level set equations and by the deterministic Monte Carlo level set equation for a sample with uniform F(t) sampling strategy 72
6-13 Comparing the level set evolution by the stochastic DO level set equations and by the deterministic Monte Carlo level set equation for a sample with random walk F(t) sampling strategy 73

6-14 Comparing the level set evolution by the stochastic DO level set equations and by the deterministic Monte Carlo level set equation for a sample with switch sample F(t) sampling strategy 74

6-15 The zero level set contours obtained from DO-MC Gamma and deterministic Monte Carlo simulation are compared using Frechet Distance as a fraction of grid spacing. The contour in red is from Monte Carlo simulation and contour in black is from DO-MC simulation 75

6-16 The zero level set contours obtained from DO-MC Gamma and deterministic Monte Carlo simulation are compared using Frechet Distance as a fraction of grid spacing. The contour in red is from Monte Carlo simulation and contour in black is from DO-KL Gamma simulation . 76

6-17 The zero level set contours obtained from DO-MC Gamma and deterministic Monte Carlo simulation are compared using Frechet Distance as a fraction of grid spacing. The contour in red is from Monte Carlo simulation and contour in black is from DO-Taylor Gamma simulation 77

7-1 Double Gyre Flow field used in the simulation for Energy Optimal Path Planning. The figure shows snapshots at various times during the simulation. 81

7-2 The class within which $F_{\mathrm{DO}}(t;r)$ is sampled for energy optimal path planning in a double gyre flow 82

7-3 Exploring the energy utilized by a vehicle in traveling from start point (0.2,0.2) to reach a target at (0.6,0.6). The time to reach the target is obtained from our new stochastic DO level-set equations. 83

7-4 Two paths that reach between T=0.049 and T=0.052 but the path shown in right panel uses 32% less energy than path shown in left panel 83

7-5 Two paths that reach between 0.06 and 0.09. The path on right panel, which uses a variable speed, is able to save energy 84

7-6 Two paths that use constant engine speeds. The path on the right, even though it uses the lower engine speed, takes much more time to reach and thus uses more energy. 84

7-7 The start point is marked as a circle and the end point is marked as a star. The color axis shows the depth. 86

7-8 The red path is the path for a vehicle with $F_{\max}$ and the green path is for the vehicle with $F_{\min}$. The level set contours for the both vehicles at the time at which the faster vehicle reaches the target is shown in black, overlaid on ocean currents at that time 88

7-9 The stochastic DO level-set simulations are used to explore different energy utilizations for Glider mission durations of 19 days and under, aiming to find sets of optimal energy paths within that a pre-selected stochastic class of vehicle speed time-history. 89

7-10 (a) is a path that reaches in the shortest time, 12.96 days, but consuming highest energy and (b) shows a path that takes 6 days more to complete the mission (18.78 days in total), but utilizes 40% lower energy. The vehicle speed along the path is plotted in color 89

7-11 (a) is a path that reaches in 16 days using a constant speed and (b) shows a path that takes 16 days but has an engine speed obtained from switch sampling, and this utilizes lower energy (about 10% lower) than the path which uses constant speed 90

List of Tables

6.1 Optimal Parameters for the energy optimal path arriving to the end point in optimal time T=0.26. 62
6.2 Numerical parameters in energy optimal path planning to cross a simulated steady front 63

7.1 Non-Dimensional Parameter list for Double Gyre simulation 81
7.2 Dimensional Parameter list for Double Gyre simulation 81

Chapter 1

Introduction

The use of autonomous underwater vehicles(AUVs) and underwater gliders is growing in a wide range of applications such as oil and gas exploration, ocean floor mapping, search and rescue operations, security and acoustic surveillance, and coastal and global ocean monitoring, conservation, forecast and prediction (Stommel, 1989; Bachmayer et al., 2004; Bellingham and Rajan, 2007). Ocean sampling is at the heart of many underwater operations. For coupled sampling and exploration missions being developed in recent years (e.g. Bhatta et al., 2005; Curtin and Bellingham, 2009; Bahr et al., 2009; Ramp et al., 2009; Leonard et al., 2010; Schofield et al., 2010), long endurance and low energy costs are important requirements. Specifically, there is a need to increase the capability of vehicles to operate for long periods of time at sea, often either by developing more efficient power supplies (Bellingham and Rajan, 2007) or by utilizing the environment to reduce energy consumption (Webb et al., 2001). Similar requirements arise in various other applications where the environment plays a significant role in navigation such as navigation of land robots, drones, airplanes etc. Conserving fuel by designing energy efficient paths leads to cost savings and environmental protection. In the present work, we consider the problem of finding an energy optimal path for ocean applications.

The task of designing a path for a mobile robot to navigate from start point (s) to a desired goal (f) (see Fig. 1-1) by optimizing one or more of (a) the time taken for travel, (b) energy expended, (c) data collected, and (d) vehicle safety, is called path

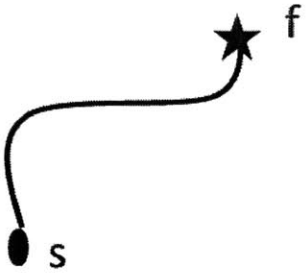

Figure 1-1: General definition of path planning is the task of designing a path for mobile robot to navigate from start point (s) to a desired goal (f) by optimizing a set of objective criterion

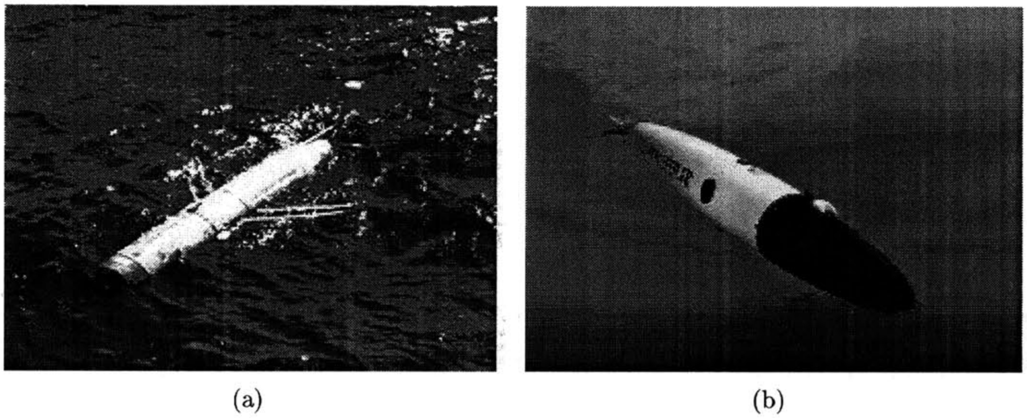
(a)
(b)

Figure 1-2: (a) is a Slocum glider (b) is SeaExplorer, a propelled AUV from ACSA ALCEN. (Wikipedia, 2012)

planning. The term path planning has different usage in various fields of science and engineering. In a general sense, it refers to the set of rules provided to an autonomous robot for navigation (Lolla et al., 2012). For a general reading of motion planning algorithms we refer the readers to Hwang and Ahuja (1992) and LaValle (2006). The problem of path planning has been studied extensively in the context of robotics [see for e.g. Sheu and Xue (1993); Latombe (1996); Kavraki et al. (1996)]. For AUV navigation, two main ocean model feedback systems are employed. The first is to use a model for forecasting the ocean flow field and use it for AUV path planning. The second is to adaptively gather ocean flow data as the vehicle navigates and perform onboard routing (Lermusiaux et al., 2014).

Typical propelled AUVs have an endurance of 12-25 hrs and speeds upto 5 knots, and typical gliders have endurance from a few days upto months and typical speeds upto 1 knot (Sherman et al., 2001; Rudnick et al., 2004; Schofield et al., 2007). Fig. 1-2 shows an image of a slocum glider and a propelled AUV. The effect of dynamic nature of ocean currents on the motion of underwater ocean vehicles is significant. The ocean currents can be comparable to the speed of AUVs (Schmidt et al., 1996; Elisseeff et al., 1999). For the motion of gliders, the ocean currents are quite often about 2-3x the glider's thrust. The energy budget of gliders depends on mission goal and environmental conditions. The largest energy expenditure for a glider is often to overcome skin friction (Eriksen et al., 2001). Here, the challenge is to develop rigorous path planning algorithms that intelligently utilize favorable currents and avoid adverse currents to increase endurance and reduce energy consumption. Also, once deployed, these vehicles often have little/no human intervention. As such, we need to design the paths of these vehicles before deployment with information about the ocean currents predicted (within predictability limit) using modern numerical ocean prediction systems.

We present the use of a rigorous partial- differential-equation-based path planning algorithm that is inspired by the level set method to determine energy optimal paths among all time optimal paths that navigate a vehicle to a target within a dynamic flow environment. The path so generated also avoids obstacles. For solving the energy optimal path planning problem, we utilize a novel model order reduction/uncertainty quantification method called Dynamically Orthogonal equations and further develop it for stochastic level-set Hamilton-Jacobi equations employed for computational design, and optimization. We test our algorithm first for two canonical steady flows that simulate a steady front and a steady eddy. Next we apply our algorithm to idealized ocean simulations with a double gyre flow and realistic ocean simulations with ocean data in the Middle-Atlantic Bight region near the New Jersey shelf/Hudson Bay.

In the next chapter we present a literature review. In chapter 3, we introduce a formal problem statement followed by a background of time optimal level set based path planning and new energy-related questions that we raise. Chapter 4 deals with the new energy optimal path planning theory that we develop in this thesis. Chapter 5 concerns the algorithms used for implementing the methodology developed in chapter 4. Chapter 6 covers canonical flows to demonstrate the method. In Chapter 7, we consider path planning in a flow field generated by an idealized double gyre model which simulates a realistic ocean jet flow. In this chapter, we also apply our theory to path planning of a glider released from Buzzard's Bay (offshore from WHOI) to reach a target in Autonomous Wide Aperture Cluster for Surveillance (AWACS) experiment region near the New Jersey Shelf/Hudson Bay. A summary and conclusions are presented in Chapter 8.

Chapter 2

Literature Review

Path planning for robotic systems have received wide attention (see for e.g. Lolla (2012) for a review). However, underwater path planning in a dynamic and unsteady ocean has been studied to a lesser extent (Lolla et al., 2014d). Various methods have been reported in literature for path planning. First we list the methods that we review. Next, we review these methods with a special focus on energy optimality for underwater vehicles.

Dynamic programming based methods like Dijkstra's method and A* search have been used for path planning. Rapidly Exploring Random Trees (RRTs) is also a popular method. These two are used in discrete domains with grid generation being a key step. In the continuous domain, algorithms have been developed using fast marching methods, and using wavefront expansions. Yet another approach is to perform a path parametrization and designing a path by optimization on these parameters. For obstacle avoidance, potential field methods have been reported. Some other algorithms use flow structures like Lagrange Coherent Structures to design navigation paths for vehicles. Another class of methods is based on formulating the path planning problem as a non-linear optimal control problem. Modified level set based method is used for rigorous time-optimal path planning. In the discussion that follows, readers are referred to relevant literature for more information about how the methods reviewed are used for other optimality (for e.g. time-optimality) and other applications (for e.g. robotic path planning).

A* approaches were applied to AUV path planning by Carroll et al. (1992); Garau et al. (2009a). The key to a successful application of A* algorithm is availability of a heuristic, and as such, there is no guarantee of optimality when extended from a discrete grid based path to a continuous path. Moreover, A* paths become infeasible in strong flows and complex environment. Garau et al. (2009b) applied the A* search based path planning algorithm in the navigation of underwater gliders surveying the Western Mediterranean sea and show that planned paths utilize substantially lower energy compared to straight line paths when ocean currents are comparable to vehicle speeds.

Rapidly Exploring Random Trees (RRTs)(Lavalle, 1998; Kuffner and LaValle, 2000) is a sampling based method used to explore the workspace for navigating a robot quickly and uniformly. RRTs have been mostly used for path planning of ground vehicles. Jaillet et al. (2010) used RRT combined with stochastic optimization to obtain minimum work path for a robot. Compared to robotic path planning, RRTs have been used in fewer application for underwater path planning. Tan et al. (2004) used RRTs for obtaining an obstacle free path for an AUV, but without considering oceanic currents. Rao and Williams (2009) used RRT for generating feasible paths of underwater gliders navigating in ocean currents. They used an A* search to identify a path from among RRT paths such that an energy based path cost heuristic which is linear in the nominal glider speed was minimized. However, the authors report that the method is not capable of identifying minimum energy paths when the flow is strong. For more information on RRT readers are referred to papers such as Bruce and Veloso (2002); Melchior and Simmons (2007); Yang et al. (2010); Karaman and Frazzoli (2011) A related method using a kinematic tree based navigation planner that is resolution complete was developed by Chakrabarty and Langelaan (2013) for UAVs in complex unsteady wind fields.

The above methods are discrete node based graph methods. For path planning in a continuous domain, fast marching methods (Sethian, 1999a) have been used. These methods are mostly applied in the context of time optimal path planning using an isotropic cost function by (Sethian, 1999b) and an extended anisotropic version by

(Petres et al., 2007). Another method for continuous domain path planning is based on wavefront expansions. These are also mostly used for time optimal path planning and hence we don't review them here. However, readers are referred to (Soulignac et al., 2009; Thompson et al., 2009, 2010) for further information.

Path parametrization and an optimization on the path parameters is another method reported in literature for AUV path planning. Alvarez et al. (2004) introduced a path parametrization in 3D (2 in space and 1 in time) and 4D (3 in space and 1 in time) to obtain candidate paths for vehicles with fixed thrust that are strictly monotone in x-coordinate. The candidate paths are then optimized through a genetic algorithm (GA) to minimize energy required to overcome the drag (which is taken as a path integral of cube of vehicle velocity). The application shown is for path planning in a simulation of Sicily channel in the Mediterranean Sea using a forecast from Harvard primitive equation model. However, GA solution is not guaranteed to converge in finite time and the assumptions might not be applicable for a complicated flow environment. Readers are referred to Chien-Chou et al. (2014) for an overview of evolutionary path planning algorithms. Kruger et al. (2007) also introduce a path parametrization in 4D (3D in space and 1D in time) and attempt to optimize a weighted cost function that accounts for energy, obstacle avoidance, time of travel and target visitation. For the energy cost function, the energy required to overcome drag (quadratic nominal velocity) and provide acceleration (rate of change of nominal velocity) is considered. Here, the authors allow for variable engine thrust and use nonlinear optimization techniques to modify each path parameter to find an energy optimal path. The authors present an example of navigation in a simulation of Hudson River around Manhattan. Even though such non-linear optimization techniques don't have drawbacks of evolutionary algorithms, the choice of parametrization affects the optimization, thereby making straightforward application to a variety of flow fields rather difficult and potentially computationally expensive. Sequential quadratic programming has also been employed by Beylkin (2008) to solve a discrete mechanics and optimal control problem of optimally finding a path for a balloon moving in windy atmosphere by optimizing a cost functional that is the l_2-norm of the control.

Potential field techniques has been used in AUV path planning (Warren, 1990) and to design robotic paths (Barraquand et al., 1992) that avoid obstacles and forbidden regions. These techniques define a potential field function that penalizes paths passing through a forbidden region. For energy based path-planning, (Witt and Dunbabin, 2008) combines potential field for avoiding obstacles and perform a swarm optimization to find minima of a energy cost function on parametrized paths. The cost function accounts for energy to overcome drag force (quadratic nominal velocity) and acceleration force (rate of change of nominal velocity). The swarm optimization is not rigorous and the authors perform refinements of an ad-hoc nature to further refine and optimize paths chosen by swarm optimization. The algorithms are tested by simulation and experimentally with Starbug AUV using pregenerated forecast data sets for Brisbane's Moreton Bay.

Lagrange Coherent Structures (LCS) have been shown to be useful for path planning (Inanc et al., 2005; Zhang et al., 2008). Specifically, the authors illustrate that the optimal energy-time-weighted paths computed by a "heuristic receding-horizon" nonlinear programming problem (NLP) method are close to paths along Lagrangian Coherent Structures (LCS). Paths are generated using B-Spline approximation of currents and a Nonlinear Trajectory Generation (NTG) software. For cost, the authors consider a weighted sum of temporal cost and energy cost (quadratic nominal velocity), and compute solutions for large/small weights of the time and energy costs. The authors then show that if paths were chosen to be along the dynamically-evolving LCSs boundaries, they would be near-optimal trajectories. The application area is Monterey bay and the flow is obtained from HF-radar (CODAR) data. For other application of collaborative tracking of LCS in a double gyre simulation, experimental flow tank, and using ocean data for Santa Barbara Channel along the California coast from Scripps, we refer readers to Hsieh et al. (2012); Michini et al. (2014).

Time optimal path planning problems can be solved as a non-linear optimal control problem (Bryson and Ho, 1975; McLain and Beard, 1998; Aghababa, 2012). Aghababa (2012) formulate a 2-point boundary value problem for energy optimal path planning by fixing a maximum time to reach, and use evolutionary algorithms to solve for a path that minimize an energy based cost function that depends on nominal velocity to the power of 3/2. Specifically the authors compare the performance of Genetic Algorithms (GA), and Ant Colony Optimization (ACO) with respect to Conjugate Gradient (CJ) methods in simple test problems.

Modified Level Set Method (Osher and Sethian, 1988; Sethian, 1999b) have been developed for time optimal path planning (Lolla, 2012; Lolla et al., 2012, 2014c,d,b,a). The authors develop a rigorous partial differential equation based path planning algorithm that generates a time optimal path in a flow field. By solving the level set equation forward in time and then a particle tracking equation backward in time, they generate a path that is time optimal for navigating underwater vehicle in unsteady moving ocean currents. Further details of time-optimal level set method is provided in chapter 3. The present thesis builds from the level set based time-optimal path planning method to develop a methodology to solve the energy optimal path planning problem.

In this chapter we reviewed the existing literature, with a focus on energy-optimal path planning for ocean applications. In the the next chapter we summarize the time optimal path planning results, ask new questions and formally state a mathematical problem statement for the present thesis.

Chapter 3

Background and Problem Statement

In this chapter we briefly describe the time optimal path planning using level set method (Lolla, 2012; Lolla et al., 2012, 2014d,b) that forms the starting point of this thesis. After summarizing path planning based on level set methods, we proceed to ask new questions that inspired our work. Then we describe the goal of this thesis and formally introduce the mathematical problem statement.

3.1 Time-Optimal Path Planning using Level Set Methods

Osher and Sethian (1988) introduced the use of level set methods as a convenient numerical framework for front evolution and tracking. The level set of a function $f(\mathbf{x}), \mathbf{x} \in \mathbb{R}^n$ is defined as the set of points at which the function takes a given constant value, i.e, it is the set $\{\mathbf{x}|f(\mathbf{x}) = C\}$, where C is a given constant. Lolla (2012) explore the novel use of the level set method for computing the reachability set for a vehicle navigating in any bounded flow field and thereby develop a new methodology for solving the time optimal path planning problem. Using generalized derivatives, Lolla et al. (2014d) provide a rigorous derivation for the new level set equation that governs the reachability front. Specifically, this time-optimal level set evolves normal to itself at a nominal (engine) speed F and gets advected by the underlying flow field $\mathbf{v}(\mathbf{x}, t)$.

The equation so developed is a Hamilton-Jacobi equation,

$$\frac{\partial \phi}{\partial t} + F|\nabla \phi| + \mathbf{v}(\mathbf{x}, t) \cdot \nabla \phi = 0 \tag{3.1}$$

and ϕ is its viscosity solution initialized with a signed distance function from the starting point. The authors prove that all points inside the zero level set contour that have $\phi < 0$ form the reachability set and the zero level set is in fact the reachability front for the vehicle traveling with nominal engine speed of F. This forms an elegant method of tracking the points reachable by a vehicle. The authors also prove that vehicles which have heading angle normal to the evolving level set travel on the time optimal path. This optimal path ($\mathbf{x}^*$), is then computed by a particle tracking equation integrated backward in time from the target using (3.2) (Lolla et al., 2014d).

$$\frac{\mathrm{d}\mathbf{x}^*}{\mathrm{d}t} = -\mathbf{v}(\mathbf{x}, t) - F\frac{\nabla \phi(\mathbf{x}, t)}{|\nabla \phi(\mathbf{x}, t)|} \tag{3.2}$$

3.2 New Questions

The above recently developed time optimal path planning theory and algorithm, combined with our new objectives of energy-optimal path planning give rise to some new questions that inspired the present thesis. The questions that we ask and address in our thesis are

1. Can energy-optimal paths in complex, strong and time-varying currents be predicted? Can it be done for all (or a given set) of arrival times?
2. Can/Should this prediction be formulated as a stochastic PDE-based design and optimization problem?
3. Can the Dynamically Orthogonal (DO) equations be utilized to efficiently solve such problems?
4. If yes, what are computational costs/advantages?
5. Are the resulting schemes usable with real ocean systems?

3.3 Goal

Consider a vehicle with instantaneous nominal (engine) speed given by F(t) navigating in a flow field $v(\mathrm{x}, t)$. The goal of the present work is to compute the optimal energy path(s) among all time-optimal paths from point A to point B (refer to Fig. 3-1).

The energy cost function to be optimized is given in terms of a power function as,

$$E = \int_0^{T(\mathbf{x_f};\mathbf{p}(\bullet))} p(t)dt \tag{3.3}$$

Importantly, our methodology allows to utilize any type of power consumption, $p(t)$, dependence with velocity. For example, for a:

- Linear Optimal, $p(t) = |F(t)|$, which is often used in control theory for explaining methodologies, see (Athans and Falb, 2006). This can correspond to a constant drag.

- Quadratic Optimal, $p(t) = F(t)^2$, also used in control theory manuscripts. This can correspond to a linear drag.

- Cubic Optimal, $p(t) = F(t)^3$. This can correspond to a quadratic drag.

Diverse power function including higher order dependence with F(t) will be illustrated in section §6.2.2.

For more realistic experiments, the power function consists of terms proportional to various forms of drags and of an acceleration term weighted adequately. For the motion of a glider that is not accelerating, most of the engine thrust expended to sustain the speed is utilized in overcoming pressure and skin drags (form drag) as well as induced drag, e.g. (Sherman et al., 2001). The total effective drag is often observed to be proportional to the square of velocity for medium Reynolds number flows and for the Slocum and Spray gliders (Rudnick et al., 2004). In the case of the Seaglider, its laminar-flow shape gives it a drag that increases as $u^{3/2}$ rather than this more common u^2 dependence.

For the power expenditure due to motions, in the present thesis, we will utilize the more common dependence and thus focus a power consumption due to glider motion in u^2. In doing so, we also assume that the total time needed for accelerations (the sum of speed-switching periods) is much smaller than the total time spent at constant speed (sum of the times spent without accelerating). In other words, the glider accelerates or decelerates from time to time, but most of the time, it operates at a constant speed and we can thus ignore the acceleration costs and only consider a cost of the form: $\int F(t)^p dt$.

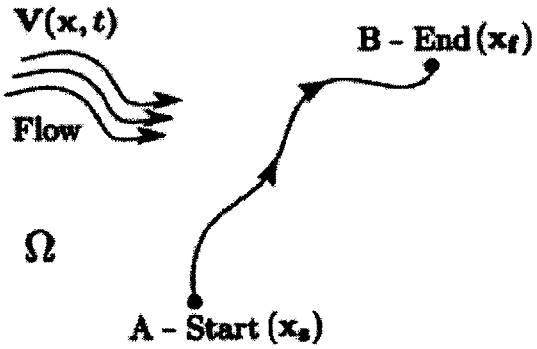

Figure 3-1: Goal of the present work is to compute the energy optimal path(s) among all the time optimal paths from point A to point B (Lolla et al., 2012).

3.4 Time-Optimal Path Planning using the level-set Hamilton Jacobi equation: provided time dependent engine speed

Before providing a statement of the problem that we solve, we obtain a relatively straightforward extension of the HJ level-set equation (3.1) for the situation where the engine speed is provided but time-dependent, i.e. the relative vehicle speed F(t) is given and variable. In that case, the viscosity solution of the Hamilton-Jacobi level-set equation with the time-dependent speed, i.e.

$$\frac{\partial \phi}{\partial t} + F(t)|\nabla \phi| + \mathbf{v}(\mathbf{x}, t) \cdot \nabla \phi = 0 \tag{3.4}$$

provides the reachability front and the time optimal path is obtained by a backtracking equation,

$$\frac{\mathrm{d}\mathbf{x}^*}{\mathrm{d}t} = -\mathbf{v}(\mathbf{x},t) - F(t)\frac{\nabla\phi(\mathbf{x},t)}{|\nabla\phi(\mathbf{x},t)|} \tag{3.5}$$

Let us consider a time $t > 0$, where the vehicle has a reachability set and front. From this instance, the vehicle travels at an instantaneous nominal (engine) speed $F(t)$ for a time interval *dt*. The reachability front (i.e. the zero level set) evolves normal to itself with the instantaneous $F(t)$. The reachability front still remains optimal for this $F(t)$. For backtracking, the heading angle is normal to the zero level set, which at the instant t, is independent of the instantaneous $F(t)$, and hence the same for all $F(t)$. For two different $F(t)$, the only difference is the rate at which the reachability front evolves normal to itself. Hence, for a given and variable $F(t)$, the solution of equation (3.4) is time-optimal.

3.5 Problem Statement

The problem statement can be formulated as follows.

Let $\Omega \in \mathbb{R}^n$ be an open set. Consider a vehicle with instantaneous nominal speed $F(t) \geq 0$ navigating from $\mathbf{x_s}$ to $\mathbf{x_f}$ (Fig. 3-1); the solution domain is $(\mathbf{x},t) \in \Omega \times (0,\infty)$. The vehicle heading is chosen such that it reaches $\mathbf{x_f}$ using $F(t)$ in optimal time. This implies that all selected paths satisfy (3.4). Hence, we seek a $F(\bullet)$ that minimizes the energy cost function. i.e.

$$\min_{F(\bullet)} \int_0^{T(\mathbf{x_f};F(\bullet))} p(t)dt \tag{3.6a}$$

$$\text{s.t.}\frac{\partial\phi(\mathbf{x},t)}{\partial t} = -F(t)|\nabla\phi(\mathbf{x},t)| - \mathbf{v}(\mathbf{x},t)\cdot\nabla\phi(\mathbf{x},t) \tag{3.6b}$$

$$\text{in } (\mathbf{x},t) \in \Omega \times (0,\infty)$$

$$T(\mathbf{x_f};F(\bullet)) = \min_{t(\mathbf{x_f};F(\bullet))}\{\phi(\mathbf{x_f},t(\mathbf{x_f};F(\bullet))) < 0\} \tag{3.6c}$$

$$\phi(\mathbf{x_s},0) = 0 \tag{3.6d}$$

$$\phi(\mathbf{x},0) = |\mathbf{x} - \mathbf{x_s}| \tag{3.6e}$$

$$F(t) \geq 0 \tag{3.6f}$$

$$p(\bullet) = F(\bullet)^n, \qquad \text{where } n = 2 \tag{3.6g}$$

For any $F(\bullet)$, based on the result obtained in section §3.4, solving for the viscous solution of (3.6b) with initial conditions given by (3.6d)-(3.6f) until the time given by (3.6c), and then solving the backtracking equation (3.5), we obtain the continuous-time history of time-optimal vehicle heading angles, $\theta^*(t)$. These headings guarantee time-optimality for the particular choice of continuous-time history of engine speed, $F(t)$, chosen. Then, among all such time optimal paths which reach the target using $F(\bullet)$, we seek to find an optimum $F(\bullet)$ that minimizes the energy required (3.6a).

Remark 1: As $F(\bullet)$ decreases, on the one hand $p(\bullet)$ decreases, but on the other hand, $T(\mathbf{x_f}; F(\bullet))$ increases. Hence, for some arbitrary choice of two $F(\bullet)$, we could get the same $T(\mathbf{x_f}; F(\bullet))$, but very different energy consumption, and the above optimization problem will choose the lowest energy $F(\bullet)$ design.

Remark 2: The opposite effect of changing $F(\bullet)$ on the total time to reach and total energy used, gives rise to a Pareto Front as used in cooperative game theory (LaValle and Hutchinson, 1998). We show results in Chapter 6. Such a behavior gives the vehicle operator freedom to choose an energy optimal path that completes a mission in a given time frame.

Remark 3: In the present thesis, we will focus on $p(t) = F(t)^2$. However, we also provide examples for other power functions in §6.2.2. The methodology developed is directly usable for all cases.

3.6 Conclusion

In this chapter we first presented the background of time-optimal path planning using level set method. We then laid out the questions that inspired the present thesis, provided the goal of the current work and explained an extension of the time-optimal path planning methodology to the time-optimal path planning in the case of variable F(t). Finally, we stated the problem statement formally and concluded with some remarks. In the next chapter, we outline the theory/methodology that we developed to solve the energy optimal path planning problem stated in this chapter.

Chapter 4

Methodology

4.1 Introduction

Different approaches can be considered for solving the energy optimal path planning problem developed in the previous chapter (equation (3.6)). One approach is to consider the problem as an optimal control problem and use the solution for two point boundary value problem to find an energy optimal paths (Athans and Falb, 2006). However, such schemes are often inefficient for time-dependent flow and most schemes are heuristic in nature (see for e.g. Aghababa (2012)).

A second approach for solving the energy optimal path planning problem is to use heuristic deterministic optimization. Here, starting from a certain type of $F(t)$ or control (e.g. bang-bang, reduced function space), a heuristic refinement process (e.g. Bisection method) can be used to update the $F(t)$ to iteratively reach an optimum or approximate optimum for that class of $F(t)$. This process is intrinsically heuristic and it can be an inefficient step-by-step search without a guarantee of full optimality. A better approach would compute the optimal or near-optimal solutions within a class or certain type of $F(t)$ all at once.

Hence, another method for solving the energy optimal path planning problem setup is to use stochastic optimization. In this approach, we consider the $F(t)$ in equation (3.4) as a random variable. This $F(t)$, then acts as an external stochastic forcing to the level set equations, rendering it stochastic level set equation. Ideally, if the stochastic PDE can be solved at once for a given class of stochastic $F(t;\omega)$, then the solution for that class is obtained, which would be an advantage when compared to a step-by-step search. However, it is only for a comprehensive sampling of $F(t;\omega)$ in a class of functionals that the stochastic optimization would yield the truly optimal solution for a large class of $F(t)$. The sampling can be done for $F(t;\omega)$ from a probabilistic distribution (e.g. Uniform distribution), or a stochastic process (e.g. random-walk or a more general suitable markov process). The advantage of this method is that if it is feasible, the solution within the class would be found in a single, albeit possibly expensive, stochastic optimization step. Of course, if the class within which the search is performed is complete, one would get the true solution. If the class is not complete, one can utilize the optimal result obtained for a given class to hierarchically generate new classes from the existing ones, hence refining the optima at each stochastic optimization, aiming to obtain the true solution for a complete class iteratively. This hierarchical stochastic optimization is an accelerated heuristic deterministic optimization in the sense that a class of $F(t;\omega)$ is evaluated at each step, instead of a single $F(t;\omega)$.

However, a disadvantage of this stochastic optimization approach is the possible expensive cost of solving the stochastic PDEs. Fortunately, we can exploit the non-linearities of fluid flows and investigate if the stochastic level-set equations could be solved with a Dynamically Orthogonal decomposition (Sapsis and Lermusiaux, 2009).

Based on the above discussion, for the present thesis, we will focus on developing and applying a new stochastic optimization methodology to solve the energy optimal path planning problem using new dynamically orthogonal level set equations and an optimization algorithm on the stochastic simulation output.

4.2 Stochastic Optimization Setup

Considering the nominal engine speed as a random variable, $F(t;\omega)$, we obtain the stochastic level set equation written in the Langevin form

$$\frac{\partial\phi(\mathbf{x},t;\omega)}{\partial t} = -F(t;\omega)|\nabla\phi(\mathbf{x},t;\omega)| - \mathbf{v}(\mathbf{x},t)\cdot\nabla\phi(\mathbf{x},t;\omega) \tag{4.1}$$

in the domain given by

$$(\mathbf{x},t) \in \Omega \times (0,\infty);\ \omega \text{ is random event.} \tag{4.2}$$

We solve the SPDE until the first time instant $T(\mathbf{x_f};F(\bullet;\omega))$ which satisfies

$$\phi(\mathbf{x_f},T(\mathbf{x_f};F(\bullet;\omega));\omega) < 0 \tag{4.3}$$

using the initial and boundary conditions given by

$$\phi(\mathbf{x_s},0;\omega) = 0 \tag{4.4}$$

$$\phi(\mathbf{x},0;\omega) = |\mathbf{x}-\mathbf{x_s}| \tag{4.5}$$

$$\frac{\partial^2\phi(\mathbf{x},t;\omega)}{\partial\mathbf{x}^2}\Big|_{\delta\Omega} = 0 \tag{4.6}$$

and non-negative nominal engine speeds,

$$F(t;\omega) \geq 0. \tag{4.7}$$

Such a stochastic simulation, gives us the distribution of time to reach $T(\mathbf{x_f};F(\bullet;\omega))$ for a externally forced distribution of $F(\bullet;\omega)$. An optimization is performed for each simulated time to reach, to obtain the $F^*(\bullet)$ that minimizes the energy objective function for that time to reach. This can be expressed mathematically in terms of an integral of power function as

$$E(F(\bullet;\omega),T) = \int_0^{T(\mathbf{x_f};F(\bullet;\omega))} p(t)dt \tag{4.8}$$

$$F^*(t) = \underset{F(\bullet;\omega)}{\arg\min}\, E(F(\bullet;\omega), T) \tag{4.9}$$

As discussed in section §3.3, some typical power functions are:

$$\begin{aligned} p(t) &\sim F(t) \quad &(4.10)\\ p(t) &\sim F(t)^2 \quad &(4.11)\\ p(t) &\sim F(t)^3 \quad &(4.12)\end{aligned}$$

where (4.10) is a power function that results in a constant grad (also called fuel optimal in some cases), (4.11) results in a linear drag optimal path, and (4.12) results in a quadratic drag energy optimal path.

The most straightforward method to solve the SPDE is through a Monte Carlo (MC) simulation of deterministic simulations of the level set PDE for different realizations of $F(t;\omega)$. Unfortunately, the MC solution is expensive to compute and its cost increases with number of realizations. Since in (4.1), $\mathbf{v}(\mathbf{x},t)$ is the flow field velocity, and we consider ocean applications, an efficient solution method for solving (4.1) would be a methodology that exploits the nonlinearities of the flow, which tend to concentrate the ϕ responses into specific dynamic patterns. Such a methodology is the DO decomposition (Sapsis and Lermusiaux, 2009, 2012; Ueckermann et al., 2013). However, this has never been done before for the viscosity solution of (4.1) and we will thus employ the MC solution to benchmark and evaluate our novel DO-level-set solution.

4.3 Dynamically Orthogonal Equations

For general stochastic continuous field $\phi(\mathbf{x},t;\omega)$, described by a stochastic partial differential equation (SPDE),

$$\frac{\partial\phi(\mathbf{x},t;\omega)}{\partial t} = \mathcal{L}[\phi(\mathbf{x},t;\omega),\mathbf{x},t;\omega]\,, \tag{4.13}$$

Sapsis and Lermusiaux (2009) applied a generalized dynamic Karhunen-Loeve (KL) decomposition

$$\phi(\mathbf{x},t;\omega) = \bar{\phi}(\mathbf{x},t) + \sum_{i=0}^{s} Y_i(t;\omega)\tilde{\phi}_i(\mathbf{x},t) \tag{4.14}$$

and an orthogonality condition on the evolution of stochastic subspace

$$\langle \frac{\partial \tilde{\phi}_i}{\partial t}, \tilde{\phi}_j \rangle = 0 \qquad \forall\, i,j \tag{4.15}$$

to obtain dynamically orthogonal equations for the statistical mean, coefficients and modes as

$$\begin{aligned} \frac{\partial \bar{\phi}(\mathbf{x},t)}{\partial t} &= \mathbb{E}[\mathcal{L}]; & (4.16)\\ \frac{\partial Y_i(t;\omega)}{\partial t} &= \langle \mathcal{L} - \mathbb{E}[\mathcal{L}], \tilde{\phi}_i \rangle; & (4.17)\\ \frac{\partial \tilde{\phi}_i(\mathbf{x},t)}{\partial t} &= \sum_{j=1}^{s} C_{ij}^{-1} \Gamma_{\tilde{\phi}}^{\perp} \mathbb{E}[Y_j \mathcal{L}]\,, & (4.18) \end{aligned}$$

where $\Gamma_{\tilde{\phi}\perp}$ is the operator which returns the component orthogonal to the stochastic subspace spanned by $\tilde{\phi}$.

Details of this work are explained in Sapsis and Lermusiaux (2009), Sapsis and Lermusiaux (2012), and Ueckermann et al. (2013). The DO equations are able to efficiently represent uncertainty in an evolving subspace.

4.4 Stochastic Simulation

To derive new DO Level Set equations we introduce a DO representation for $F(t;\omega)$, and $\phi(\mathbf{x},t;\omega)$. For brevity of notation, in the DO equations $(\mathbf{x},t;\omega)$ is dropped, the notation $\bar{\bullet}$ refers to the mean of a quantity and $\tilde{\bullet}$ refers to the mode of quantities. And in addition Y refers to the stochastic coefficients of ϕ while z refers to the coefficients of F. The subscript 'i' refers to the 'i'th coefficient or 'i'th mode as the case maybe. Hence, we have,

$$F = \bar{F} + z\tilde{F} \tag{4.19}$$

and

$$\phi = \bar{\phi} + Y_i \tilde{\phi}_i \tag{4.20}$$

as DO representations of F and ϕ. These time-dependent representations of the stochastic process $F(t)$ and ϕ are such that if truncated to a subspace of size s_F and s, respectively, each of them capture the most of these processes in the sense of variance explained (K-L property). We also have by definitions, $\mathbb{E}(z) = 0$ and $\mathbb{E}(y_i) = 0$. Substituting these into the stochastic level set equation (4.1), we get,

$$\frac{\partial \bar{\phi}}{\partial t} + Y_i \frac{\partial \tilde{\phi}_i}{\partial t} + \tilde{\phi}_i \frac{\mathrm{d}Y_i}{\mathrm{d}t} = -(\bar{F} + z\tilde{F}) \left| \nabla(\bar{\phi} + Y_i \tilde{\phi}_i) \right| - \mathbf{v} \cdot \nabla(\bar{\phi} + Y_i \tilde{\phi}_i) \tag{4.21}$$

To derive the mean, mode and coefficient equations from (4.21), we need to pay special attention to the non-polynomial, non-linearity in the SPDE, viz., $\left|\nabla(\bar{\phi} + Y_i \tilde{\phi}_i)\right|$. Some approaches are reported in literature in (Debusschere et al., 2005; Julier and Uhlmann, 1996) for based model order reduction schemes based on the polynomial chaos expansion. Next, we propose different approaches to evaluate (or find an approximation to) this term. Each approach leads to new DO equations and they are described in the following sections. For ease of bookkeeping, we introduce a new notation for the non-polynomial non-linearity as,

$$\gamma \equiv |\nabla \phi| \tag{4.22}$$

For 2-dimensions in space we have,

$$\gamma = \sqrt{\frac{\partial \phi}{\partial x}^2 + \frac{\partial \phi}{\partial y}^2} \tag{4.23}$$

and for 3-dimensions in space we have,

$$\gamma = \sqrt{\frac{\partial \phi}{\partial x}^2 + \frac{\partial \phi}{\partial y}^2 + \frac{\partial \phi}{\partial z}^2} \tag{4.24}$$

We will focus mainly on 2D in space applications, but that the equations that follow are applicable to applications in larger dimensions.

Hence, (4.21) becomes

$$\frac{\partial \bar{\phi}}{\partial t} + Y_i \frac{\partial \tilde{\phi}_i}{\partial t} + \tilde{\phi}_i \frac{\mathrm{d}Y_i}{\mathrm{d}t} = -(\bar{F} + z\tilde{F})\gamma - \mathbf{v} \cdot \nabla(\bar{\phi} + Y_i \tilde{\phi}_i) \tag{4.25}$$

In addition to the analytical derivations and methodological aspects involved in reducing (4.25) to the DO decompositions, we mention the need of paying attention to numerical properties for stochastic viscosity solutions and their applications to these new DO equations for (4.25). These will be outlined in section §5.3. Next, we focus only on the analytical equations.

4.4.1 DO-MC Gamma

The first approach we consider is to evaluate the non-polynomial non-linearity (γ) through a Monte Carlo computation without evoking a separate DO representation for γ. This approach will not fully exploit the redundancy in γ that can be obtained through a stochastic reduced order representation. Nonetheless, we exploit redundancy in ϕ which leads, as we illustrate, to substantial cost savings. The mean, mode and realization evolution equations for this approach are

$$\begin{aligned}
\frac{\partial \bar{\phi}}{\partial t} &= -(\bar{F}\mathbb{E}[\gamma] + \mathbb{E}[z\gamma]\tilde{F}) - \mathbf{v} \cdot \nabla \bar{\phi} && (4.26)\\
\frac{\mathrm{d}Y_i}{\mathrm{d}t} &= -\left\langle \bar{F}(\gamma - \mathbb{E}[\gamma]) + \tilde{F}(z\gamma - \mathbb{E}[z\gamma]) + Y_k \mathbf{v} \cdot \nabla \tilde{\phi}_k, \tilde{\phi}_i \right\rangle && (4.27)\\
\frac{\partial \tilde{\phi}_i}{\partial t} &= -C^{-1}_{Y_iY_j}(\bar{F}\mathbb{E}[Y_j\gamma] + \tilde{F}\mathbb{E}[zY_j\gamma]) + \mathbf{v} \cdot \nabla \tilde{\phi}_i \\
&\quad -\left\langle -C^{-1}_{Y_iY_j}(\bar{F}\mathbb{E}[Y_j\gamma] + \tilde{F}\mathbb{E}[zY_j\gamma]) + \mathbf{v} \cdot \nabla \tilde{\phi}_i, \tilde{\phi}_n \right\rangle \tilde{\phi}_n && (4.28)
\end{aligned}$$

4.4.2 DO-KL Gamma

The second approach we consider is to introduce a DO representation for the non-polynomial non-linearity (γ) as

$$\gamma = \bar{\gamma} + \alpha_i \tilde{\gamma}_i \tag{4.29}$$

where α_i and $\tilde{\gamma}_i$ and coefficients and modes respectively for reduced order representation for γ. The number of modes for representing γ (s_γ) and ϕ (s) can in general be different. By inserting (4.29) into (4.21), we obtain the mean, coefficient and mode equations as

$$\begin{aligned}
\frac{\partial \bar{\phi}}{\partial t} &= -(\bar{F}\bar{\gamma} + \tilde{F}\mathbb{E}[z\alpha_i])\tilde{\gamma}_i - \mathbf{v} \cdot \nabla \bar{\phi} && (4.30) \\
\frac{\mathrm{d}Y_i}{\mathrm{d}t} &= -\left\langle (\bar{F}\alpha_k + z\tilde{F}\alpha_k - \bar{F}\mathbb{E}[\alpha_k] - \tilde{F}\mathbb{E}[z\alpha_k])\tilde{\gamma}_k + Y_k \mathbf{v} \cdot \nabla \tilde{\phi}_k + z\tilde{F}\bar{\gamma}, \tilde{\phi}_i \right\rangle && (4.31) \\
\frac{\partial \tilde{\phi}_i}{\partial t} &= -C^{-1}_{Y_iY_j}(\mathbb{E}[Y_j\alpha_k]\tilde{\gamma}_k\bar{F} + C_{Y_jz}\tilde{F}\bar{\gamma} + \mathbb{E}[Y_jz\alpha_k]\tilde{\gamma}_k\tilde{F}) - \mathbf{v} \cdot \nabla \tilde{\phi}_i && (4.32) \\
&\quad - \left\langle -C^{-1}_{Y_iY_j}(\mathbb{E}[Y_j\alpha_k]\tilde{\gamma}_k\bar{F} + C_{Y_jz}\tilde{F}\bar{\gamma} + \mathbb{E}[Y_jz\alpha_k]\tilde{\gamma}_k\tilde{F}) - \mathbf{v} \cdot \nabla \tilde{\phi}_i, \tilde{\phi}_n \right\rangle \tilde{\phi}_n
\end{aligned}$$

The challenge of this approach is to arrive at an expression for the mean, modes and coefficients of γ. We consider two methods for overcoming this challenge.

SVD for Gamma

The mean, mode and coefficients are obtained by a reduced order SVD of γ realizations computed from ϕ realizations. i.e.

$$\bar{\gamma} = \mathbb{E}[\left|\nabla(\bar{\phi} + Y_i\tilde{\phi}_i)\right|] \tag{4.33}$$

We define a matrix of mean removed γ^r realizations,

$$M \equiv \begin{bmatrix} \left|\nabla(\bar{\phi} + Y_i^1\tilde{\phi}_i)\right| - \bar{\gamma} & \left|\nabla(\bar{\phi} + Y_i^2\tilde{\phi}_i)\right| - \bar{\gamma} & \cdots & \left|\nabla(\bar{\phi} + Y_i^m\tilde{\phi}_i)\right| - \bar{\gamma} \\ \vdots & \vdots & \vdots & \vdots \end{bmatrix} \tag{4.34}$$

where the superscript on Y_i refers to realization number and m is the number of realizations.

By taking an SVD of the matrix of realizations, we obtain,

$$\begin{aligned}
M &= U * S * V^T && (4.35) \\
\alpha &= V * S^T && (4.36)
\end{aligned}$$

$$\tilde{\gamma} = U \tag{4.37}$$

Dimensionality reduction is achieved by choosing the first s_γ columns of U as the modes $\tilde{\gamma}$.

Taylor for Gamma

A DO/KL representation of the non-polynomial non-linearity can be obtained by applying a Taylor series expansion of the realizations around $\bar{\phi}$. Such a Taylor series expansion gives us an expression for $\bar{\gamma}$, α and $\tilde{\gamma}$ needed in equations (4.30) to (4.33) as,

$$\bar{\gamma} = \sqrt{\bar{\phi}_x^2 + \bar{\phi}_y^2} \tag{4.38}$$

$$\alpha_i = Y_i \tag{4.39}$$

$$\tilde{\gamma}_i = \tilde{\phi}_{i_x} \frac{\bar{\phi}_x}{\sqrt{\bar{\phi}_x^2 + \bar{\phi}_y^2}} + \tilde{\phi}_{i_y} \frac{\bar{\phi}_y}{\sqrt{\bar{\phi}_x^2 + \bar{\phi}_y^2}} \tag{4.40}$$

where the subscript x and y refer to derivatives with respect to x and y (Osher and Sethian, 1988)

4.4.3 Comments/Remarks

The DO coefficient equation can be integrated in time by a MC algorithm in the DO subspace (Ueckermann et al., 2013). Hence, the DO method which is generally used for uncertainty quantification can be used as a computationally efficient stochastic optimization technique.

An alternative way to look at the approaches to handle non-polynomial non-linearity is from the point of view of algorithms. For the time integration of the mean, mode and coefficient equations a computational estimate of the mean, mode and coefficient for γ is required. The different approaches described above provide a method for making this computation. In the SVD for Gamma approach (§4.4.2), the modes are estimated by a reduced order SVD. However, in practice computing an SVD at each time step has a cost $O(mn^2)$ where m is the number of samples and n is the number of grid points which can become computationally time consuming for large problems. A lanczos method or a Krylov subspace method can reduce the computational effort to $O(ns^2)$ (Gugercin, 2005), where s is the size of the DO subspace. As we are only interested in obtaining an approximation for the modes, it is sufficient to update the modes of γ intermittently. An intermittent SVD computation is faster than an algorithm which requires SVD computation at every time step, but produces good approximate results as we will show in §6.4.1.

The algorithm view point of the Taylor for Gamma method is that the mean, mode and coefficients for the non-polynomial non-linearity are approximated by a first order Taylor expansion. This approximation gives good results as long as the pdf of the γ function is well approximated by a locally linear representation. Since the pdf of γ depends on the pdf of the level sets governed by the sample path eqn (4.1) and on the pdf of the gradient of level set realizations, this approximation can be good but not in all cases. This is illustrated in section §6.4.1.

4.5 Optimization

The second part of solving the energy optimal path planning problem is to perform an optimization of $E(F(\bullet,\omega),T)$ (refer to equation (4.8)) of the stochastic samples such that some constraints of $T(x_f;\omega)$ are met.

The new stochastic DO-level set equations provide, for each of the sample of $F(t;\omega)$ considered, the optimal time-to-reach the target. Thus, in terms of DO representation, the optimization becomes,

$$F_{\text{DO}}(t;r) = \bar{F} + z(t;r)\tilde{F} \tag{4.41}$$

$$F^*_{\text{DO}}(t) = \arg \min_{F_{\text{DO}}(\bullet;r)} \int_0^{T(\mathbf{x_f};F_{\text{DO}}(\bullet;r))} F_{\text{DO}}(t;r)^2 dt \tag{4.42}$$

Other power functions can be used as described in §3.3

4.6 Brief Derivations

4.6.1 DO-MC Gamma Derivation

In this section, we present the new DO level set equations introduced in §4.4 and briefly describe their derivation.

We first derive equations (4.26) to (4.28). Starting from the level set SPDE given by (4.1), substituting the DO expansions for F and ϕ, we obtain,

$$\frac{\partial\bar{\phi}}{\partial t} + Y_i\frac{\partial\tilde{\phi}_i}{\partial t} + \tilde{\phi}_i\frac{\mathrm{d}Y_i}{\mathrm{d}t} = -(\bar{F} + z\tilde{F})\gamma - \mathbf{v}\cdot\nabla(\bar{\phi} + Y_i\tilde{\phi}_i) \tag{4.43}$$

The mean equation is obtained by taking expectation on both sides of (4.43)

$$\frac{\partial\bar{\phi}}{\partial t} = -(\bar{F}\mathbb{E}[\gamma] + \tilde{F}\mathbb{E}[z\gamma]) - \mathbf{v}\cdot\nabla\bar{\phi} \tag{4.44}$$

The coefficient equation is obtained by taking an inner product of (4.43) with the modes and applying the dynamically orthogonal condition,

$$\left\langle\frac{\partial\bar{\phi}}{\partial t},\tilde{\phi}_n\right\rangle + Y_i\left\langle\frac{\partial\tilde{\phi}_i}{\partial t},\tilde{\phi}_n\right\rangle + \left\langle\tilde{\phi}_i,\tilde{\phi}_n\right\rangle\frac{\mathrm{d}Y_i}{\mathrm{d}t} - \left\langle\bar{F}\gamma - \tilde{F}z\gamma,\tilde{\phi}_n\right\rangle - \left\langle\mathbf{v}\cdot\nabla\bar{\phi} - Y_i\mathbf{v}\cdot\nabla\tilde{\phi}_i,\tilde{\phi}_n\right\rangle \tag{4.45}$$

First term on the LHS of (4.45) is obtained by taking an inner product of (4.44) with modes,

$$\left\langle\frac{\partial\bar{\phi}}{\partial t},\tilde{\phi}_n\right\rangle = -\left\langle(\bar{F}\mathbb{E}[\gamma] + \tilde{F}\mathbb{E}[z\gamma]) + \mathbf{v}\cdot\nabla\bar{\phi},\tilde{\phi}_n\right\rangle \tag{4.46}$$

Substituting (4.46) into (4.45) we have

$$\overset{0,\,\text{DO condition}}{\cancel{Y_i\left\langle\frac{\partial\tilde{\phi}_i}{\partial t},\tilde{\phi}_n\right\rangle}} + \left\langle\tilde{\phi}_i,\tilde{\phi}_n\right\rangle\frac{\mathrm{d}Y_i}{\mathrm{d}t} = -\left\langle\bar{F}(\gamma - \mathbb{E}[\gamma]) + \tilde{F}(z\gamma - \mathbb{E}[z\gamma]) + Y_i\mathbf{v}\cdot\nabla\tilde{\phi}_i,\tilde{\phi}_n\right\rangle \tag{4.47}$$

$$\frac{\mathrm{d}Y_i}{\mathrm{d}t} = -\left\langle\bar{F}(\gamma - \mathbb{E}[\gamma]) + \tilde{F}(z\gamma - \mathbb{E}[z\gamma]) + Y_k\mathbf{v}\cdot\nabla\tilde{\phi}_k,\tilde{\phi}_i\right\rangle \tag{4.48}$$

(4.47) to (4.48) is because of orthogonality of modes.

Multiplying on both sides of (4.43) by the coefficients and taking expectation we have

$$Y_j\frac{\partial\bar{\phi}}{\partial t}+Y_jY_i\frac{\partial\tilde{\phi}_i}{\partial t}+\tilde{\phi}_iY_j\frac{dY_i}{dt}=-(Y_j\gamma\bar{F}+zY_j\gamma\tilde{F})-Y_j\mathbf{v}\cdot\nabla\bar{\phi}-Y_jY_i\mathbf{v}\cdot\nabla\tilde{\phi}_i \tag{4.49}$$

$$C_{Y_jY_i}\frac{\partial\tilde{\phi}_i}{\partial t}+\tilde{\phi}_iC_{Y_j\frac{dY_i}{dt}}=-\bar{F}\mathbb{E}[Y_j\gamma]-\tilde{F}\mathbb{E}[zY_j\gamma]-C_{Y_jY_i}\mathbf{v}\cdot\nabla\tilde{\phi}_i \tag{4.50}$$

$C_{Y_j\frac{dY_i}{dt}}$ is obtained by multiplying (4.48) with coefficients and taking expectation as,

$$Y_j\frac{dY_i}{dt}=-\langle(Y_j\gamma-Y_jE[\gamma])\bar{F},\tilde{\phi}_i\rangle-\langle(zY_j\gamma-Y_jE[z\gamma])\tilde{F},\tilde{\phi}_i\rangle-Y_jY_k\langle\mathbf{v}\cdot\nabla\tilde{\phi}_k,\tilde{\phi}_i\rangle \tag{4.51}$$

$$C_{Y_j\frac{dY_i}{dt}}=-\langle E[Y_j\gamma]\bar{F},\tilde{\phi}_i\rangle-\langle E[zY_j\gamma])\tilde{F},\tilde{\phi}_i\rangle-C_{Y_jY_k}\langle\mathbf{v}\cdot\nabla\tilde{\phi}_k,\tilde{\phi}_i\rangle \tag{4.52}$$

Substituting (4.52) into (4.50) we get the evolution equation for modes

$$\begin{aligned}\frac{\partial\tilde{\phi}_i}{\partial t}&=-C^{-1}_{Y_iY_j}E[Y_j\gamma]\bar{F}-C^{-1}_{Y_iY_j}E[zY_j\gamma]\tilde{F}-\mathbf{v}\cdot\nabla\tilde{\phi}_i\\&-\langle(-C^{-1}_{Y_iY_j}E[Y_j\gamma]\bar{F}-C^{-1}_{YikY_j}E[zY_j\gamma]\tilde{F}-\mathbf{v}\cdot\nabla\tilde{\phi}_i),\tilde{\phi}_n\rangle\tilde{\phi}_n\end{aligned} \tag{4.53}$$

4.6.2 DO-KL Gamma Derivation

We now show the key steps required to arrive at equations (4.30) to (4.33). Introducing a DO expansion for γ in (4.43) we obtain the SPDE,

$$\begin{aligned}\frac{\partial\bar{\phi}}{\partial t}+Y_i\frac{\partial\tilde{\phi}_i}{\partial t}+\tilde{\phi}_i\frac{dY_i}{dt}&=-(\bar{F}+z\tilde{F})(\bar{\gamma}+\alpha_i\tilde{\gamma}_i)-\mathbf{v}\cdot\nabla(\bar{\phi}+Y_i\tilde{\phi}_i)\\&=-(\bar{F}\bar{\gamma}+\bar{F}\alpha_i\tilde{\gamma}_i+z\tilde{F}\bar{\gamma}+z\alpha_i\tilde{\gamma}_i\tilde{F})-\mathbf{v}\cdot\nabla(\bar{\phi}+Y_i\tilde{\phi}_i)\end{aligned} \tag{4.54}$$

We then obtain the mean equation by taking expectation of (4.54) as,

$$\frac{\partial\bar{\phi}}{\partial t}=-(\bar{F}\bar{\gamma}+\tilde{F}\mathbb{E}[z\alpha_i]\tilde{\gamma}_i)-\mathbf{v}\cdot\nabla\bar{\phi} \tag{4.55}$$

To obtain the coefficient equation we start by taking an inner product of (4.54) with the modes $\tilde{\phi}$ as,

$$\left\langle \frac{\partial \bar{\phi}}{\partial t}, \tilde{\phi}_n \right\rangle + Y_i \left\langle \frac{\partial \tilde{\phi}_i}{\partial t}, t \right\rangle + \left\langle \tilde{\phi}_i, \tilde{\phi}_n \right\rangle \frac{\mathrm{d}Y_i}{\mathrm{d}t} = -\left\langle \bar{F}\bar{\gamma} + \bar{F}\alpha_i\tilde{\gamma}_i + z\tilde{F}\bar{\gamma} + z\tilde{F}\alpha_i\tilde{\gamma}_i, \tilde{\phi}_n \right\rangle - \left\langle \mathbf{v}\cdot\nabla\bar{\phi} + Y_i\mathbf{v}\cdot\nabla\tilde{\phi}_i, \tilde{\phi}_n \right\rangle \tag{4.56}$$

The first term of LHS of (4.56) can be obtained by taking an inner product of (4.55) with $\tilde{\phi}$ as

$$\left\langle \frac{\partial \bar{\phi}}{\partial t}, \tilde{\phi}_n \right\rangle = -\left\langle \bar{F}\bar{\gamma} + \tilde{F}\mathbb{E}[z\alpha_i]\tilde{\gamma}_i + \mathbf{v}\cdot\nabla\bar{\phi}, \tilde{\phi}_n \right\rangle \tag{4.57}$$

Substituting (4.57) in (4.56) and using the dynamical orthogonality condition we have,

$$\left\langle \tilde{\phi}_i, \tilde{\phi}_n \right\rangle \frac{\mathrm{d}Y_i}{\mathrm{d}t} = -\left\langle \bar{F}\alpha_i\tilde{\gamma}_i + \tilde{F}z\bar{\gamma} + \tilde{F}(z\alpha_i - \mathbb{E}[z\alpha_i])\tilde{\gamma}_i + Y_i\mathbf{v}\cdot\nabla\tilde{\phi}_i, \tilde{\phi}_n \right\rangle \tag{4.58}$$

Using the orthogonality of modes, we then obtain the coefficient equation as,

$$\frac{\mathrm{d}Y_i}{\mathrm{d}t} = -\left\langle \bar{F}\alpha_k\tilde{\gamma}_k + \tilde{F}z\bar{\gamma} + \tilde{F}(z\alpha_k - \mathbb{E}[z\alpha_k])\tilde{\gamma}_k + Y_k\mathbf{v}\cdot\nabla\tilde{\phi}_k, \tilde{\phi}_i \right\rangle \tag{4.59}$$

For the mode equation, an expectation of (4.54) multiplied with coefficients Y_j is taken to get,

$$C_{Y_jY_i}\frac{\partial \tilde{\phi}_i}{\partial t} + \tilde{\phi}_i C_{Y_j\frac{dY_i}{dt}} = -\mathbb{E}[Y_j\alpha_i]\tilde{\gamma}_i\bar{F} - C_{Y_jz}\tilde{F}\bar{\gamma} - \mathbb{E}[Y_jz\alpha_i]\tilde{\gamma}_i\tilde{F} - C_{Y_jY_i}\mathbf{v}\cdot\nabla\tilde{\phi}_i \tag{4.60}$$

$C_{Y_j\frac{\mathrm{d}Y_i}{\mathrm{d}t}}$ is obtained by multiplying (4.59) with Y_j and taking an expectation as,

$$C_{Y_j\frac{dY_i}{dt}} = -\left\langle \bar{F}\mathbb{E}[Y_j\alpha_k]\tilde{\gamma}_k + \tilde{F}\mathbb{E}[Y_jz\alpha_k]\tilde{\gamma}_k + C_{Y_jY_k}\mathbf{v}\cdot\nabla\tilde{\phi}_k + C_{Y_jz}\tilde{F}\bar{\gamma}, \tilde{\phi}_i \right\rangle \tag{4.61}$$

Substituting (4.61) in (4.60) and rearranging, we obtain the mode equation as

$$\begin{aligned}\frac{\partial\tilde{\phi}_i}{\partial t} &= -C^{-1}_{Y_iY_j}(\mathbb{E}[Y_j\alpha_k]\tilde{\gamma}_k\bar{F} + C_{Y_jz}\tilde{F}\bar{\gamma} + \mathbb{E}[Y_jz\alpha_k]\tilde{\gamma}_k\tilde{F}) - \mathbf{v}\cdot\nabla\tilde{\phi}_i \qquad (4.62)\\ &\quad - \left\langle -C^{-1}_{Y_iY_j}(\mathbb{E}[Y_j\alpha_k]\tilde{\gamma}_k\bar{F} + C_{Y_jz}\tilde{F}\bar{\gamma} + \mathbb{E}[Y_jz\alpha_k]\tilde{\gamma}_k\tilde{F}) - \mathbf{v}\cdot\nabla\tilde{\phi}_i, \tilde{\phi}_n\right\rangle \tilde{\phi}_n\end{aligned}$$

4.6.3 DO-Taylor Gamma Derivation

In this section, we present the first order Taylor approximation for the non-polynomial non-linearity and describe the key steps in deriving results presented in §4.4.2. We consider the non-polynomial non-linearity as a function of realizations of spatial derivatives as,

$$f(\phi_x, \phi_y) = \sqrt{\phi_x^2 + \phi_y^2} \qquad (4.63)$$

Hence we have a function on which we apply a first order Taylor approximation,

$$\begin{aligned}\gamma &= f(\phi_x, \phi_y) && (4.64)\\ &= f(\bar{\phi}_x + Y_i\tilde{\phi}_{i_x}, \bar{\phi}_x + Y_i\tilde{\phi}_{i_y}) && (4.65)\\ &= f(\bar{\phi}_x, \bar{\phi}_y) + Y_i\left(\tilde{\phi}_{i_x}\frac{\partial f(\bar{\phi}_x, \bar{\phi}_y)}{\partial\bar{\phi}_x} + \tilde{\phi}_{i_y}\frac{\partial f(\bar{\phi}_x, \bar{\phi}_y)}{\partial\bar{\phi}_y}\right) && (4.66)\end{aligned}$$

Comparing:

$$\begin{aligned}\bar{\gamma} &= f(\bar{\phi}_x, \bar{\phi}_y) && (4.67)\\ \alpha_i &= Y_i && (4.68)\\ \tilde{\gamma}_i &= \tilde{\phi}_{i_x}\frac{\partial f(\bar{\phi}_x, \bar{\phi}_y)}{\partial\bar{\phi}_x} + \tilde{\phi}_{i_y}\frac{\partial f(\bar{\phi}_x, \bar{\phi}_y)}{\partial\bar{\phi}_y} && (4.69)\\ \tilde{\gamma}_i &= \tilde{\phi}_{i_x}\frac{\bar{\phi}_x}{\sqrt{\bar{\phi}_x^2 + \bar{\phi}_y^2}} + \tilde{\phi}_{i_y}\frac{\bar{\phi}_y}{\sqrt{\bar{\phi}_x^2 + \bar{\phi}_y^2}} && (4.70)\end{aligned}$$

Thus we derive the results presented in §4.4.2.

4.7 Conclusion

In this chapter we obtained a methodology to solve the optimization problem through stochastic optimization. We also briefly outlined the theory of Dynamically Orthogonal equations and derived new DO Level Set Field equations. We carefully presented different approaches to handle the non-polynomial non-linearity in the Level Set Hamilton-Jacobi equations. In the next chapter we present the algorithms developed and utilized in this thesis.

Chapter 5

Algorithm

This chapter describes the algorithms developed for solving the energy optimal path planning problem using the methodology developed in Chapter 4. First, we describe the overall algorithm, then we go into details of each step. Broadly, the algorithm has a stochastic simulation part followed by an optimization part. For the stochastic simulation, we develop algorithms to solve the DO equations and for the optimization part we use well established search and sort algorithms.

5.1 Overall Algorithm

The overall algorithm has 5 major steps, the first three of which are part of stochastic simulation and last two are part of optimization. Fig. 5-1 shows the flowchart of the algorithm developed in the present thesis.

5.2 $F(t;\omega)$ sampling

The solution to the optimization problem depends critically on the stochastic $F(t;\omega)$ chosen. As noted in the theory section, we get the optimal solution within the class of $F(t;\omega)$ we search in. Moreover, if the class within which the algorithm searches is complete, we get the true solution. Therefore, a comprehensive sampling strategy for $F(t;\omega)$ becomes useful to the quality and efficiency of solution.

We consider various sampling strategies in this work. They are as follows.

1. Uniform sampling of constant engine speed
2. Bounded Gaussian Random Walk
3. Exponentially correlated random walk
4. Switch Sampling
5. Pseudo-Uniform energy sampling
6. Bang-Bang sampling

Fig. 5-2 illustrates some samples from Uniform, Bounded Gaussian Random Walk, Exponentially Correlated Random Walk and Switch Sampling strategies.

5.3 Numerical Stochastic DO-Level Set Simulation

The first part of the algorithm solves the new stochastic DO level-set equations developed in section §4.4. Next, we describe the algorithm used for the initial and boundary conditions, and advection terms.

5.3.1 Initial and boundary condition for DO equations

The start point ($\mathbf{x_s}$) is deterministically known, and so we assume there is no uncertainty initially for the level set fields. The mean level set field is initialized with a signed distance function centered with respect to the vehicle's start point. The coefficients are initialized to zero. For initializing the level set modes, we experimented with different strategies and chose the following: The slowest vehicle is evolved deterministically for first few time steps. The SVD of time snapshots of the level set field for this vehicle is chosen as the initial modes for level set field. For the first few time steps, all vehicles evolve from the same location radially outward, and the slowest vehicle captures the possible evolution of all other vehicles. If the fastest vehicle was twice as fast as the slowest vehicle, for example, then 3 time steps of the slowest vehicle will capture the first time step of the fastest vehicle, and all other vehicles will have been captured in between.

5.3.2 Numerics

An explicit first order time marching scheme is used for time integration of mean, modes and coefficients (Ueckermann et al., 2013). For advection of the level set by the underlying flow field, we employ a Total Variation Diminishing scheme (Ueckermann et al., 2013). The gradient of the level set fields are taken according to (Sethian, 1999b). For the Taylor-Gamma scheme, the derivatives of level set modes are taken according to the viscosity solution scheme of Sethian (1999b), but the upwind direction choice is made on the basis of mean level set field's upwind direction. The algorithm is developed in MATLAB using MSEAS/MIT 2.29 Finite Volume Framework (Ueckermann and Lermusiaux, 2011).

5.3.3 Various tests

Extensive tests were conducted to verify the schemes finally used and shown in this work. Several of these tests are listed in Fig. 5-3

5.4 Optimization

We use a minimum search for finding the least energy path for all DO level-set realizations and their corresponding optimal path that complete a mission in a given time interval. For obtaining a list of paths that could be used for a mission, we use MATLAB built in sort function (McKeeman and Shure, 2004) which is an efficient implementation of the quick sort algorithm (Hoare, 1962).

5.5 Conclusion

In this chapter we briefly outlined the algorithms used for implementing the methodology developed in Chapter 4.

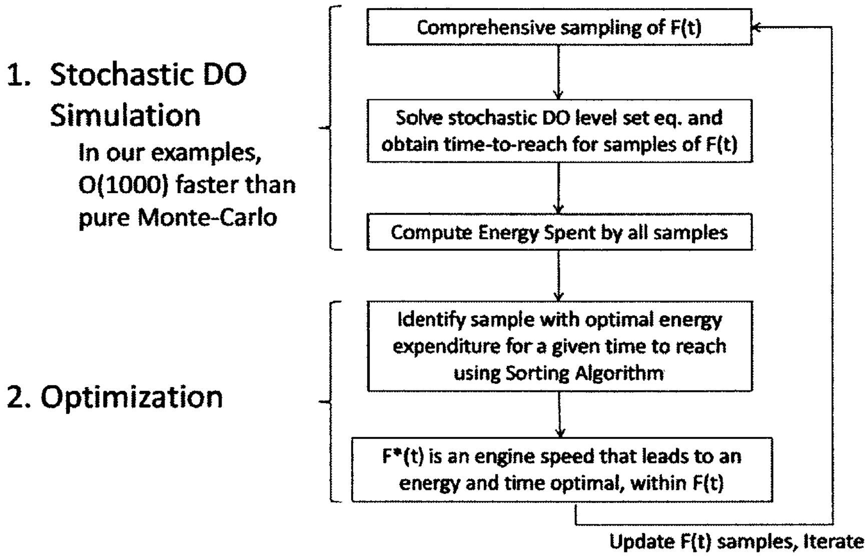
1. Stochastic DO Simulation
In our examples, O(1000) faster than pure Monte-Carlo
2. Optimization
Comprehensive sampling of F(t)
Solve stochastic DO level set eq. and obtain time-to-reach for samples of F(t)
Compute Energy Spent by all samples
Identify sample with optimal energy expenditure for a given time to reach using Sorting Algorithm
F*(t) is an engine speed that leads to an energy and time optimal, within F(t)
Update F(t) samples, Iterate

Figure 5-1: Flowchart depicting different steps of the algorithm

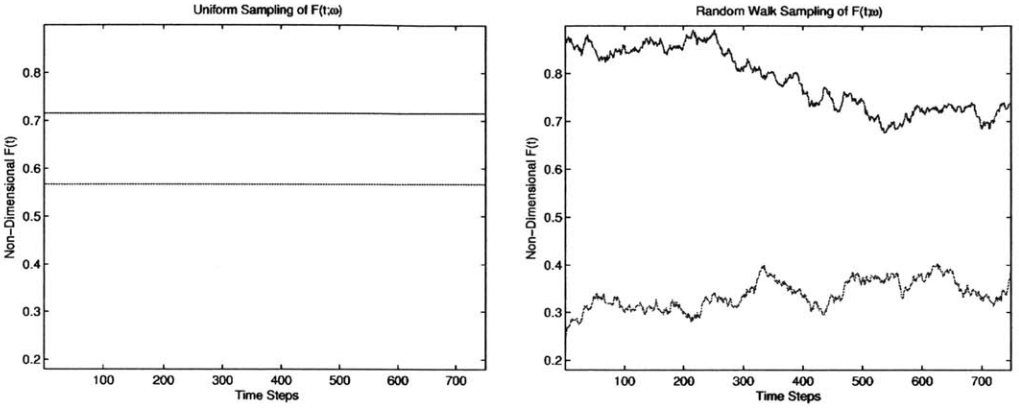

(a) Uniform Sampling

(b) Bounded Gaussian Random Walk Sampling

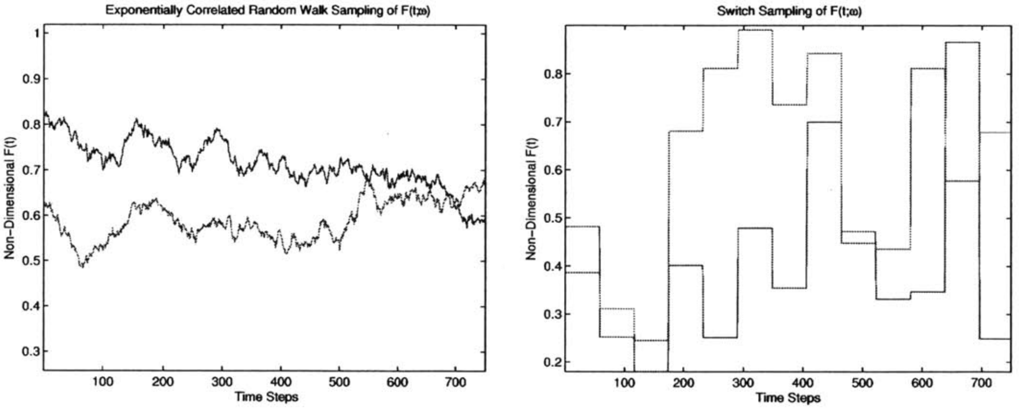

(c) Exponentially Correlated Random Walk Sampling

(d) Switch Sampling

Figure 5-2: Samples of $F(t;\omega)$ from different sampling strategies

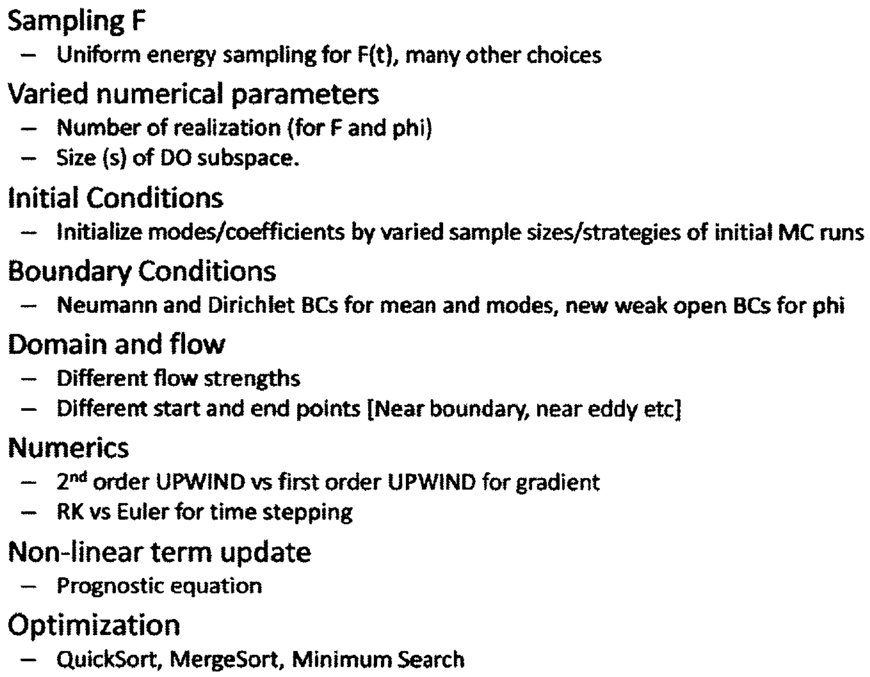

Sampling F
- Uniform energy sampling for F(t), many other choices

Varied numerical parameters
- Number of realization (for F and phi)
- Size (s) of DO subspace.

Initial Conditions
- Initialize modes/coefficients by varied sample sizes/strategies of initial MC runs

Boundary Conditions
- Neumann and Dirichlet BCs for mean and modes, new weak open BCs for phi

Domain and flow
- Different flow strengths
- Different start and end points [Near boundary, near eddy etc]

Numerics
- 2nd order UPWIND vs first order UPWIND for gradient
- RK vs Euler for time stepping

Non-linear term update
- Prognostic equation

Optimization
- QuickSort, MergeSort, Minimum Search

Figure 5-3: List of various tests performed

Chapter 6

Applications: Canonical Steady Flows

6.1 Introduction

In this chapter we present results from applying our methodology to solve energy optimal path planning problems in simple illustrative canonical flows by implementing the algorithm in MATLAB. We consider two canonical steady flows that simulate a front and an eddy. First we present a benchmark analytical solution for the simulated front, and test to see if our algorithm is able to get close to the analytical optima. Next we present an illustrative example to further illustrate the inner-workings and capabilities of the algorithm. Finally we present energy optimal path planning results for crossing a steady front, and for traveling in an eddy.

6.2 Jet flow: Simulated Steady Front

In this section, we evaluate how the algorithm performs on a simulated steady front flow. On a rectangular domain with dimensions $a \times b$, we use a jet flow to simulate a steady front as,

$$U_x = \begin{cases} U & 0.4b < x < 0.6b \\ 0 & \text{otherwise} \end{cases} \tag{6.1}$$

$$U_y = 0 \tag{6.2}$$

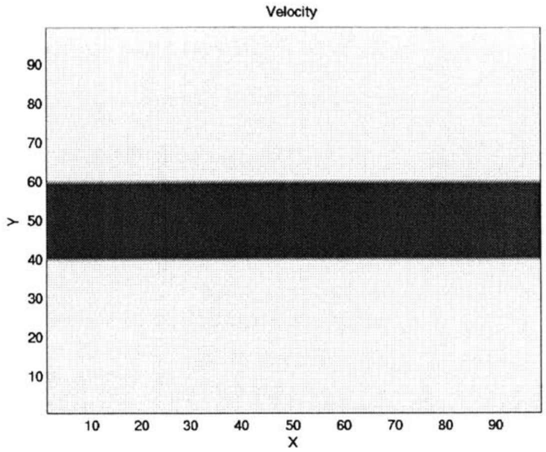

Figure 6-1: The domain with a simulated steady front used for testing and illustrating the algorithm developed in this thesis

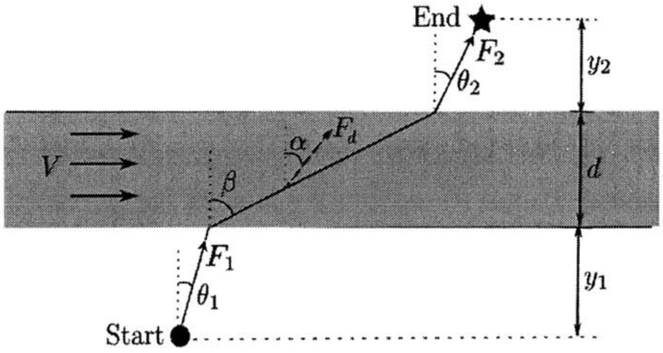

Figure 6-2: Parameters involved in optimal crossing of a jet flow: jet speed V and width d; start (circle), end (star), distances, vehicle nominal speed and headings are marked. Adapted from Lolla (2012)

where the subscripts refer to the component in that direction, and U controls the strength of the flow. The domain with the flow is shown in Fig. 6-1

6.2.1 Benchmark Solution

In this section we present an analytical solution that can be computed to serve as a benchmark to test our algorithm. Adapting the notation, we reproduce the schematic from Lolla (2012) in Fig. 6-2. Suppose we wish to determine the optimal engine operation history such that the corresponding nominal velocity of the vehicle can vary between F_{min} and F_{max} at any instant of time. The question then is to determine this nominal (relative) vehicle velocity history F(t) such that it minimizes the energy utilized while still reaching the end point in optimal time. In what follows, we provide arguments that allow us to derive a double minimization problem whose solution gives the energy-optimal in the sense defined in Section §3.5, but only for a single arrival time at a time.

To start the arguments, we first consider the motion from the start point to the highway. There, the vehicle is not affected by the environment and the level set grows normal to itself outward at a rate equal to the nominal instantaneous engine speed. The motion (e.g. total displacement over a give period) achieved by any time series of nominal engine speed is equivalent to the motion achieved by the mean nominal engine speed of that time series for the same duration. However, the energy consumption by the vehicle varies as some power function of the nominal speed that is of order higher than 1, see section §3.3. As a result, that energy consumption will be different for each time series F(t).

It can then be shown that the energy consumption to execute a motion is minimum when the mean speed is used. For illustration, suppose a vehicle travels at F_{min} for time t_1 and at F_{max} for time t_2. The motion achieved by this vehicle is equivalent to the motion achieved by a vehicle travelling at $\bar{F} = (F_{\text{min}}t_1 + F_{\text{max}}t_2)/(t_1 + t_2)$. The energy utilized by a vehicle using this particular time series is $E_v = F^p_{\text{min}}t_1 + F^p_{\text{max}}t_2$ where the subscript v refers to any vehicle. On the other hand, the energy utilized by a vehicle traveling at mean speed is $E_m = \bar{F}^n(t_1 + t_2)$. Here $n > 1$ (see for e.g. §3.3). For $n = 2$, by simple algebra we have,

$$E_m - E_v = -(\bar{F} - F_{\text{min}})(F_{\text{max}} - \bar{F}) \tag{6.3}$$

Hence we have, $E_m \leq E_v$. This can be generalized to any number of engine switch (larger than 2), using the Holder's inequality. We also note that similar arguments can be made for the vehicle motions beyond the highway up to the end point.

To continue the arguments, we now consider the motion of the vehicle within the steady and uniform jet proper, i.e. within the steady "highway", the motion of vehicle in the x-direction is affected. Here also, it can be shown that using a single speed results in lower energy consumption, and that any time series has an equivalent single time-mean speed. Therefore, an energy optimal path can only have one speed for the vehicle from the start point to the highway at some to-be-determined point, then another speed (same or different) for the time optimal motion in the highway and finally another speed for the highway to the target. This completes the arguments that allow us to set-up our double minimization problem, "energy-optimality subject to time-optimality". This is done next.

Based on the above, we assume that the optimal engine speed varies in time such that it uses F_1, F_d, and F_2 from start to the highway, within the highway, and from the start point to highway to the end point, respectively.

Let **U** denote the total effective velocity of the vehicle in the flow, as seen by a ground observer. Within the highway, we have, componentwise,

$$U_x = F_d \sin\alpha + V \tag{6.4}$$

and

$$U_y = F_d \cos\alpha \tag{6.5}$$

where U_x and U_y are the x and y components of the total vehicle velocity, **U**. This gives,

$$\tan\beta = \frac{U_x}{U_y} = \tan\alpha + \frac{V}{F_d}\sec\alpha \tag{6.6}$$

Outside of the highway, the relations are the same, but with V=0. Now, let X be the total downstream displacement of the vehicle, i.e. in the x direction. We have, from trigonometry:

$$X = y_1\tan\theta_1 + d\tan\beta + y_2\tan\theta_2 \tag{6.7}$$

Finally, the total travel time T can be written as the sum of travel times in each individual region. Hence, the time optimization problem we wish to solve is:

$$\min T = \frac{y_1}{F_1\cos\theta_1} + \frac{d}{F_d\cos\alpha} + \frac{y_2}{F_2\cos\theta_2} \tag{6.8}$$

$$\text{s.t. } X = y_1 \tan\theta_1 + d\left(\tan\alpha + \frac{V}{F_d}\sec\alpha\right) + y_2\tan\theta_2 \tag{6.9}$$

and

$$\theta_1, \theta_2, \alpha \geq 0$$

Now, on top of this time-optimality, we want to determine the energy optimal path, for each arrival time. Hence, assuming for now a general energy cost over dt as,

$$dE = p(t)dt = F(t)^n dt, \qquad \text{wheren} >= 1 \tag{6.10}$$

we obtain the energy required from this crossing of the steady front, from the start point to the end point, as:

$$E = F_1^{n-1}\frac{y_1}{\cos\theta_1} + F_d^{n-1}\frac{d}{\cos\alpha} + F_2^{n-1}\frac{y_2}{\cos\theta_2} \tag{6.11}$$

For a fixed time-to-reach the target, the optimal energy problem is formulated as,

$$\begin{aligned}
\min_{F_1,F_d,F_2} E &= F_1^{n-1}\frac{y_1}{\cos\theta_1} + F_d^{n-1}\frac{d}{\cos\alpha} + F_2^{n-1}\frac{y_2}{\cos\theta_2} && (6.12)\\
\text{s.t.} & && (6.13)\\
X &= y_1\tan\theta_1 + d\left(\tan\alpha + \frac{V}{F_d}\sec\alpha\right) + y_2\tan\theta_2 && (6.14)\\
T &= \min_{\theta_1,\alpha,\theta_2} \frac{y_1}{F_1\cos\theta_1} + \frac{d}{F_d\cos\alpha} + \frac{y_2}{F_2\cos\theta_2} && (6.15)\\
& \theta_1, \theta_2, \alpha \geq 0 && (6.16)\\
& F_{\min} \leq F_1, F_d, F_2 \leq F_{\max} && (6.17)\\
& n \geq 1 && (6.18)
\end{aligned}$$

where X, T, $F_{\min}$, and $F_{\max}$ are supplied to the optimization problem. This completes the derivation of a double minimization problem whose solution gives the energy-optimal in the sense defined in Section §3.5, but again only for a single arrival time at a time. For $y_1 = 0.2167, d = 0.2, y_2 = 0.2167, V = 3, F_{\min} = 2, F_{\max} = 3, X = 0.6334$,and importantly fixing a single target T to be $T = 0.26$ we obtain the numerical solution of our double-optimization problem as presented in Table [6.1]. This solution,

Table 6.1: Optimal Parameters for the energy optimal path arriving to the end point in optimal time T=0.26.

Parameter	Using Non-Linear Optimization	Using new stochastic DO level-set optimization
θ_1	23.19°	26.80°
θ_2	23.74°	19.53°
β	65.81°	68.43°
F_1	2.86	2.79
F_d	2.62	2.44
F_2	2.93	3.00

column 1 of Table 6.1, was computed using the iterative non-linear optimization toolbox of MATLAB.

Now, we compare this "semi-analytical" solution to the solution obtained by our new stochastic DO level-set optimization scheme. To do so, we need to select an adequate stochastic set of $F(t;\omega)$ histories. First, we remark that all vehicles will reach faster than a vehicle which travels throughout the distance at $F_{\min}$. Hence, the total time required will at most be the time required by this slowest vehicle. Let this be $T_{\max}$. The number of $F(t;\omega)$ samples, i.e. $F_{\mathrm{DO}}(t;r)$ (see equation (4.41)), required grows with the resolution in time axis exponentially, i.e., even if only two possible engine speed choices are possible, and if the time axis from 0 to $T_{\max}$ is divided into n intervals, a total of 2^n $F_{\mathrm{DO}}(t;r)$ samples are required to obtain an exhaustive search (in the bang-bang control sense). With the available computing resources and reasonable runtime, we choose to resolve the time axis into n=26 intervals. The energy optimal path planning is then performed using our new stochastic DO level set equations with this $F_DO(t;r)$ class of speed histories, i.e. an exhaustive sample space but only for that 2 speed and 26 time-intervals (25 speed switches). The result of this stochastic DO level-set optimization with the same parameters as above is presented in Table [6.1]

Table 6.2: Numerical parameters in energy optimal path planning to cross a simulated steady front

Description	Parameter	Value
Size of domain in x direction	a	100
Size of domain in y direction	b	100
Number of grids in x direction	N_x	100
Number of grids in y direction	N_y	100
Spatial discretization in x direction	dx	1
Spatial discretization in y direction	dy	1
Total time of simulation	T	1
Time step	dt	0.2
Number of DO modes	s	20
Number of DO samples	m	10000

6.2.2 Illustration of the algorithm

In this section, we use another steady flow as an example to illustrate the algorithm that was developed in this thesis. A 100 km x 100 km domain is discretized with a 1 km spatial grid. A jet flow is used to simulate a steady front that travels from left to right of the domain between y = 40 km and y = 60 km with a strength of 83 cm/s. The numerical parameters used are provided in Table [6.2]. With the stochastic DO level-set approach, a key to finding the true optima is to use an efficient and representative sample of $F(t;\omega)$ used in the stochastic DO simulation, $F_{\mathrm{DO}}(t;r)$ given in equation (4.41).

In this section, we are going to compare 3 sampling strategies. The first one is a uniform distribution for $F_{\mathrm{DO}}(t;r)$. This is used simply for comparison with the other two since it is not trying to be energy optimal since $F_{\mathrm{DO}}(t;r)$=constant in time. Hence, it should give results that will use at least as much energy than energy-optimal paths.

For the second sampling strategy, we employ a bounded gaussian random walk.

For the third sampling strategy, we are inspired from the analytical solution given in §6.2.1 and we employ a randomized switching sampling strategy. The vehicle is assumed to be able to operate at any instantaneous nominal engine speed $F(t;\omega)$ such that $5\ cm/s \leq F(t;\omega) \leq 25\ cm/s$. For discretizing this $F(t;\omega)$ representation efficiently in time, we allow switching to happen randomly in time, and at each instant the nominal engine speed is uniformly distributed between 5 cm/s and 25 cm/s. With sufficiently high number of samples, we are able to obtain a good representation of $F(t;\omega)$. $F_{\text{DO}}(t;r)$ samples for the three sampling strategies are plotted in Fig. 6-3.

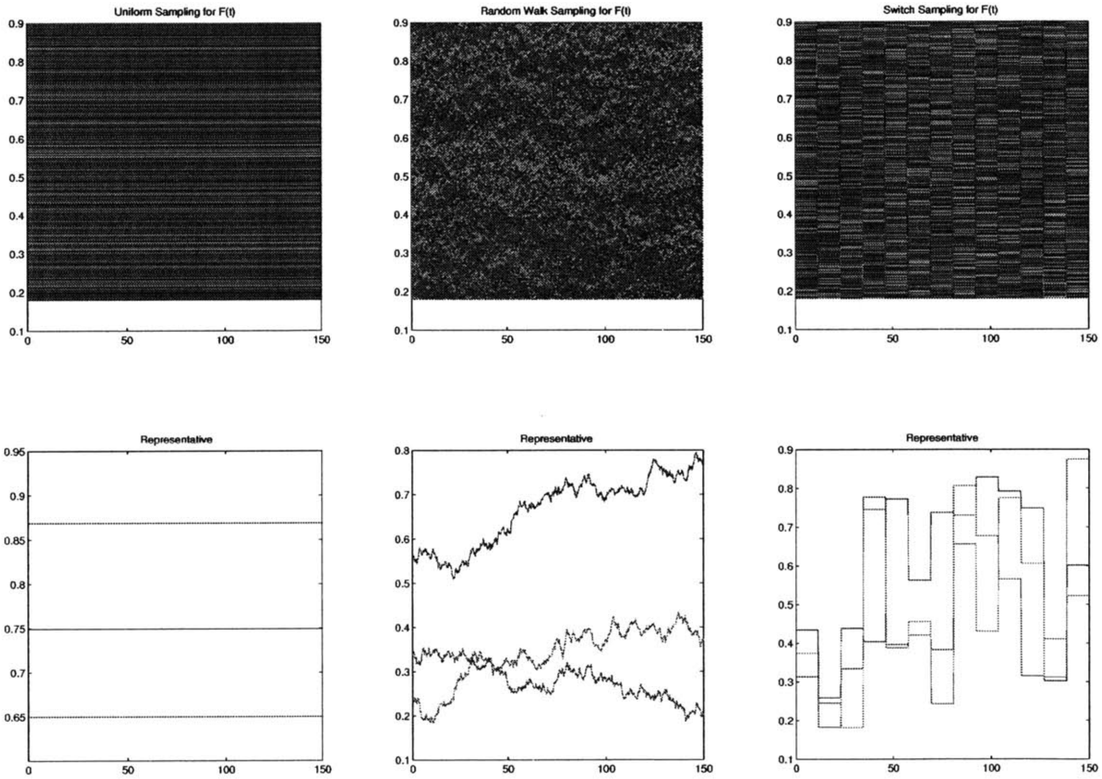

Figure 6-3: $F_{\text{DO}}(t;r)$ samples using different strategies. In the first row, we show all 10,000 samples of $F_{\text{DO}}(t;r)$ used for optimal Steady Front Crossing Path Planning. In the second row, we show representative $F_{\text{DO}}(t;r)$ samples for clarity.

Fig. 6-4 shows the zero level set evolution for samples with slowest ($F_{\min}$), fastest ($F_{\max}$), and an intermediate nominal engine speed. Zero level set of all samples will be located spatially within the zero level sets of slowest and fastest samples. The new stochastic DO-Level Set Equations evolve the zero level set of a large number of samples by evolving the mean, modes and coefficients of level set fields. In this illustration we use 30,000 samples; 10,000 of them sampled from a uniform distribution between $F_{\min}$ and $F_{\max}$, another 10,000 sampled from a Bounded Gaussian Random Walk bounded between $F_{\min}$ and $F_{\max}$, and another 10,000 from a switch sampling strategy. After the simulation, all 30,000 samples reach the end point and we get 30,000 times to reach. From the $F(t)$ samples and corresponding time to reach, we can obtain schematics such as that of Fig. 6-5 which compares the results of the stochastic optimization for different energy cost function, which depend on various powers of F in the energy expenditure $dE = F(t)^n dt$ (3.3).

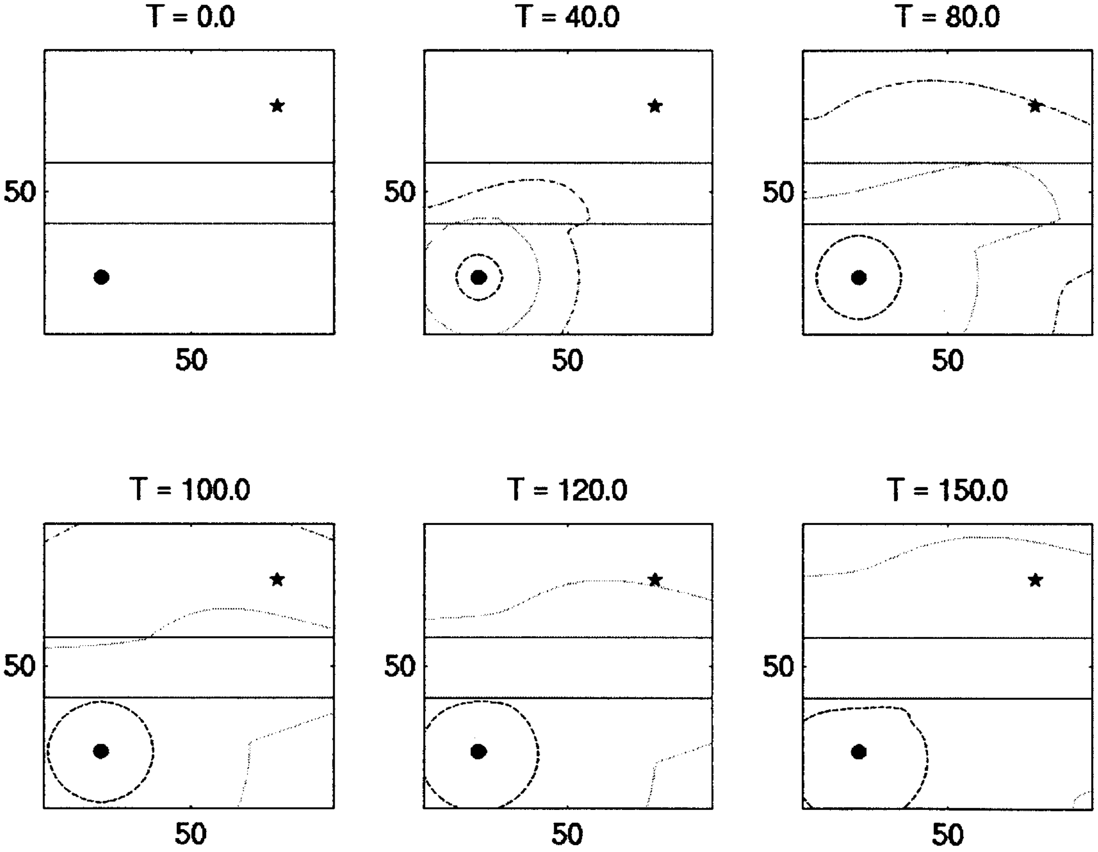

Figure 6-4: Figure shows the evolution of zero level set contours for vehicles (samples) with slowest ($F_{\min}$), fastest ($F_{\max}$), and an intermediate nominal engine speeds. We see that the slowest vehicle travelling at 5cm/s is not able to cross the steady front within 150 hrs. Zero level set of all samples will be located spatially within the zero level sets of slowest and fastest samples.

In Fig. 6-6 we used a power function that depends on square of nominal engine speed, which we will adopt in this thesis hereafter. We note that, all the methodology

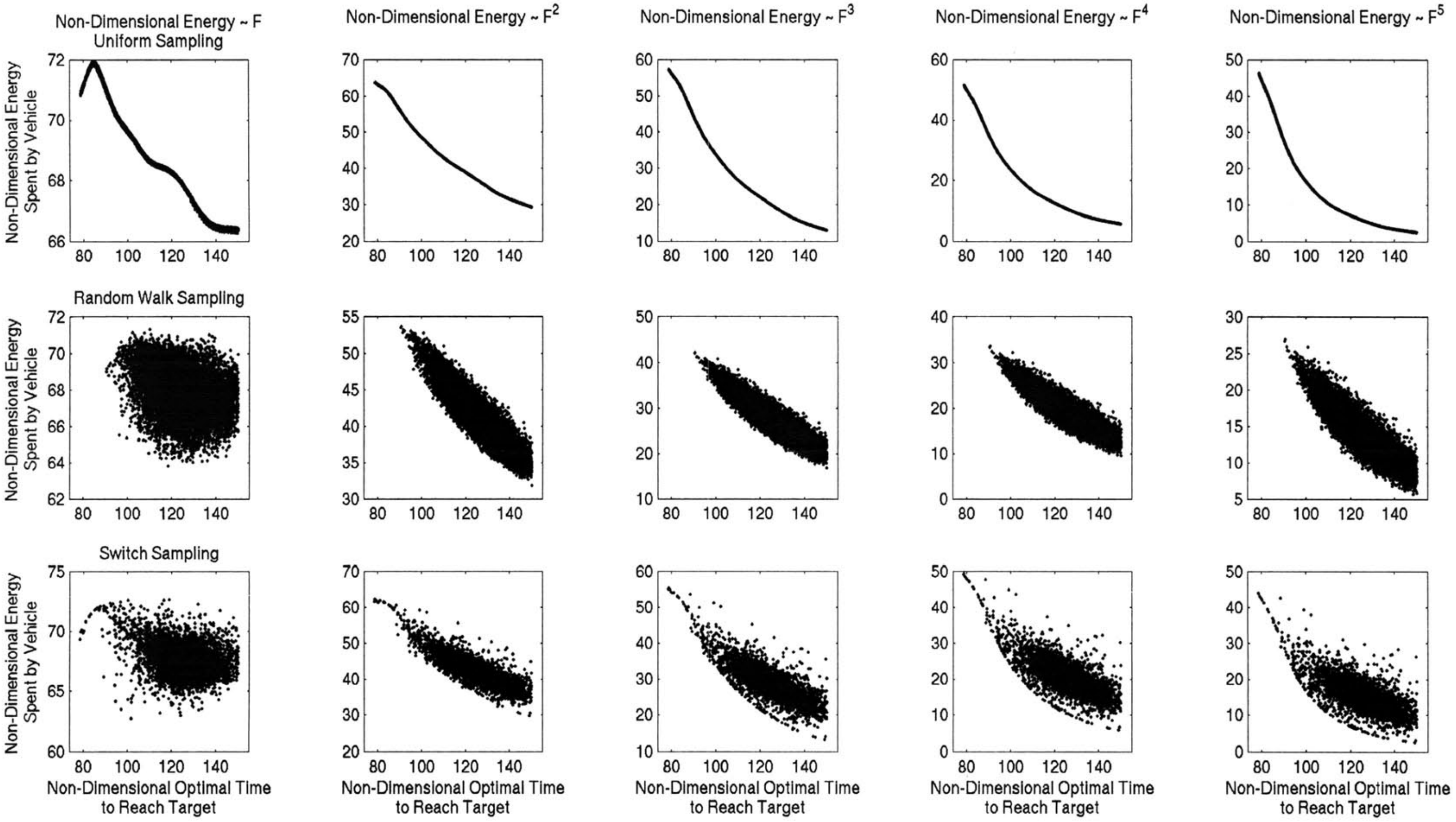

Figure 6-5: Figure shows Energy Cost Function vs Time using different power functions of nominal engine speed $F(t)$.

we developed in this thesis is directly applicable to any form of cost function, the choice of power function only enters during the optimization phase of the algorithm. For a time to reach of $T = 104.6$ we show the optimal engine speed obtained in the three classes of sampling, and that obtained by non-linear optimization in Fig. 6-7. The paths for vehicles which follow the within class energy optimal nominal engine speed is shown in Fig. 6-8. Comparison with double minimization will be completed in future work.

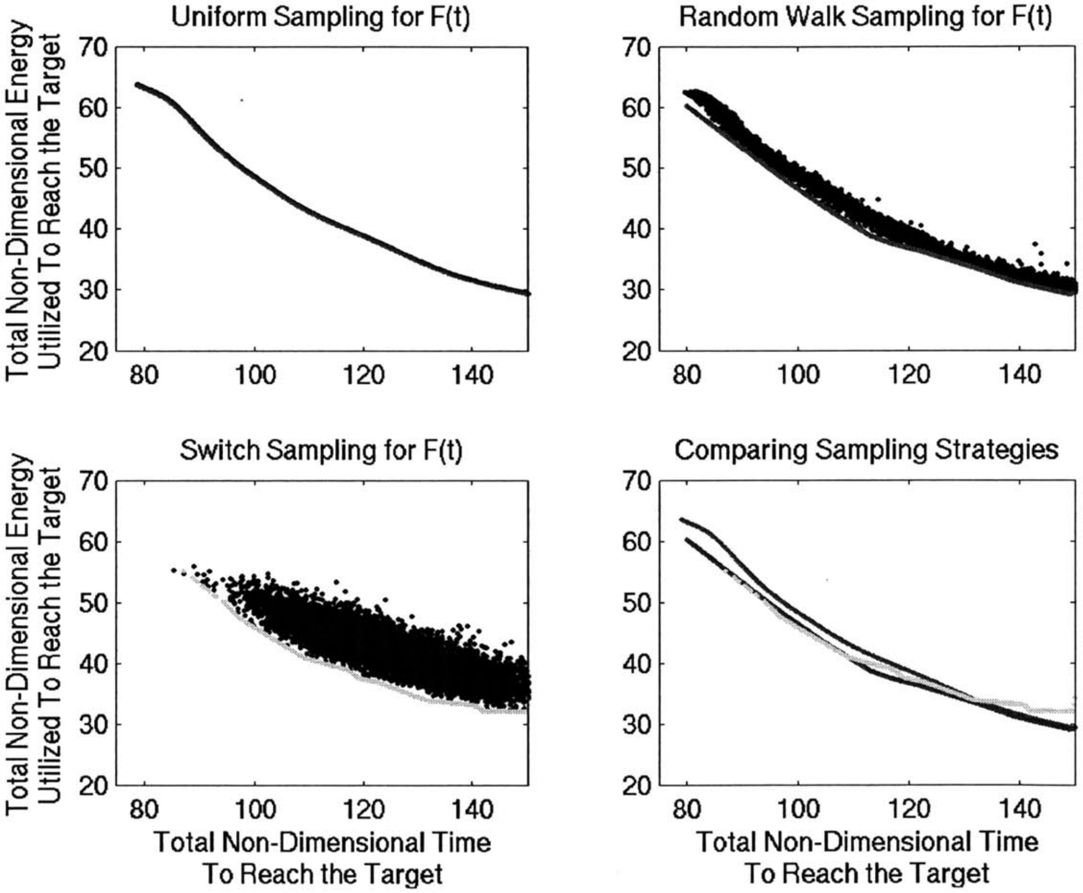

Figure 6-6: Figure shows Energy Cost Function vs Time for 30,000 (10,000 ×3) samples. The figure shows the optimal energy envelop obtained by each sampling strategy. We note that vehicles (samples) which vary the engine speed on their steady front crossing mission have energy requirements lower than those vehicles which use single engine speed for the mission. The algorithm is able to identify such nominal engine speed design which results in optimal energy for the mission paths in the class of F(t) sampling.

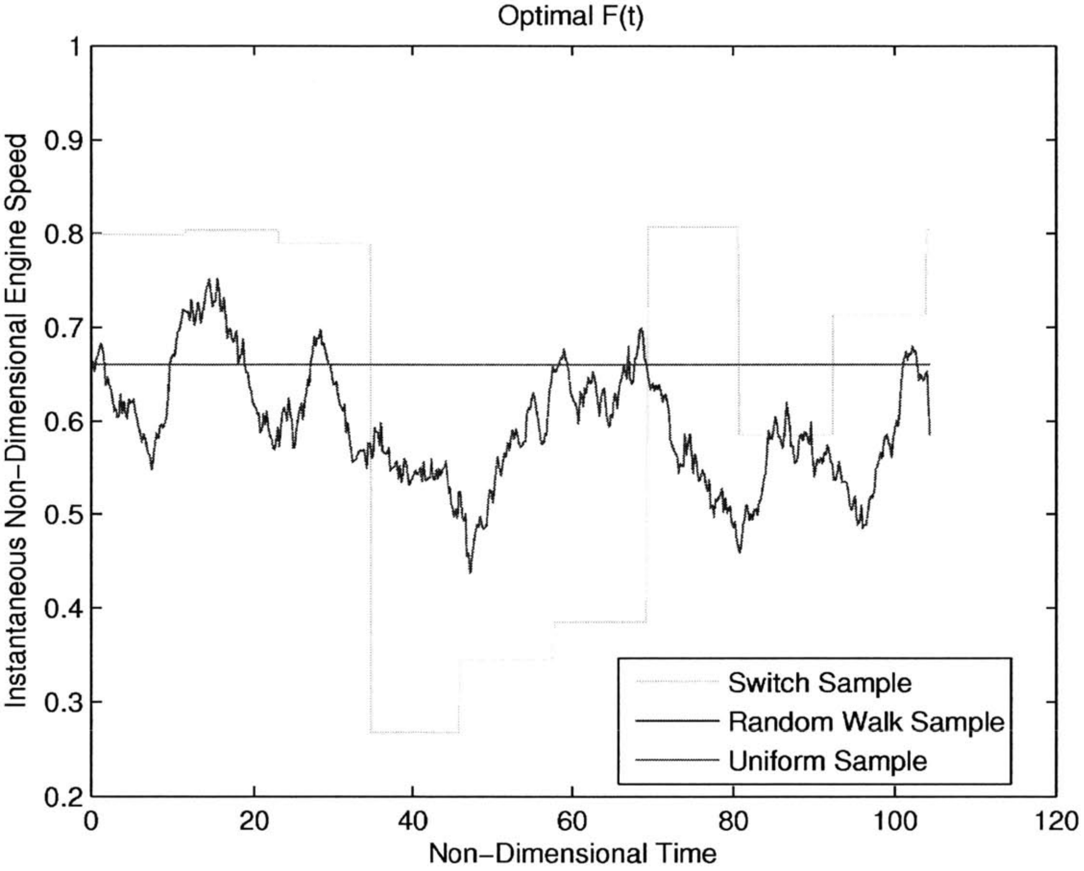

Figure 6-7: For a time to reach of $t = 104.6$ we show the optimal engine speed obtained in the three classes of sampling

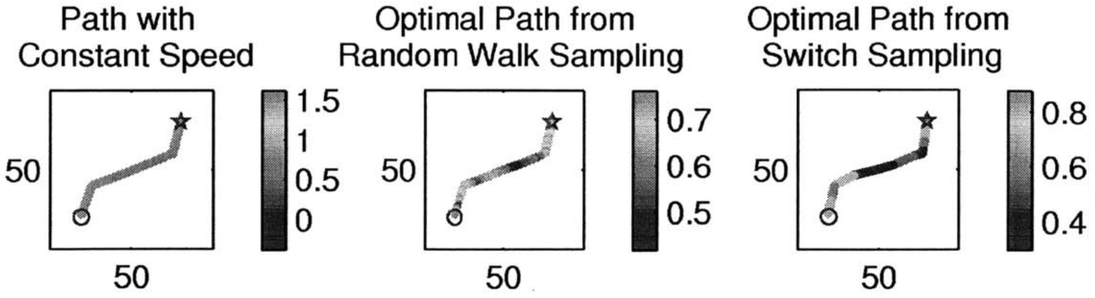

Figure 6-8: For a time to reach of $t = 104.6$ we show the optimal paths compared to the path which uses constant speed

6.3 Steady Circular Flow

In this section, we evaluate how the algorithm performs on a simulated vortex flow. On a rectangular domain with dimensions $a \times b$, we use a circular flow given by,

$$U_x = -U \cos(\pi y/b) \sin(\pi x/a) \tag{6.19}$$

$$U_y = U \sin(\pi y/b) \cos(\pi x/a) \tag{6.20}$$

where the subscripts refer to the component in that direction, and U controls the strength of the flow. The circular flow is a mathematically well behaved canonical flow that can be used to test and develop algorithms. It simulates an idealized eddy in the ocean.

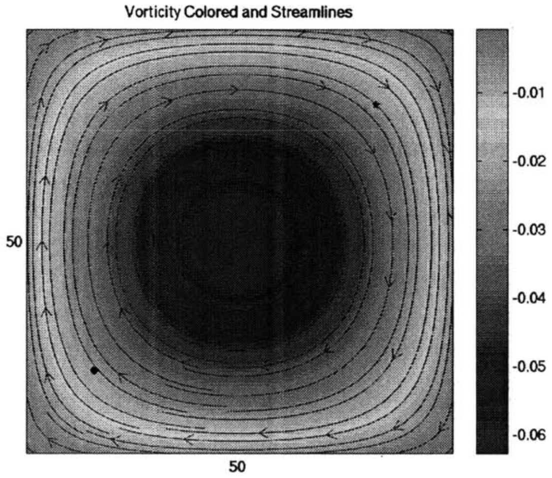

Figure 6-9: The flow field for steady circular flow

6.3.1 Energy optimal Path Planning

The new stochastic DO-level set optimization methodology is applied to the canonical circular flow and the energy utilization is explored in Fig. 6-10. The paths obtained for a selected time to reach of T=90 are shown in Fig. 6-11.

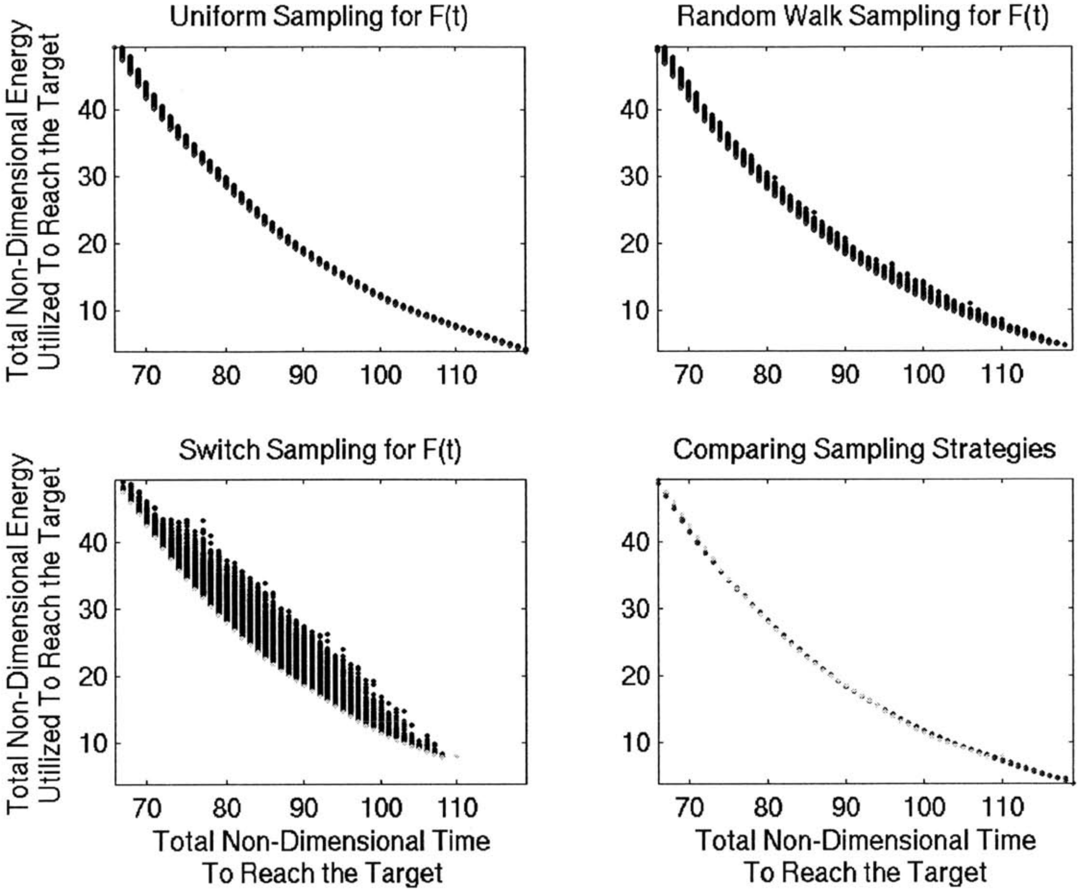

Figure 6-10: Using three stochastic DO level-set simulations for exploring energy utilization by vehicles in a circular flow

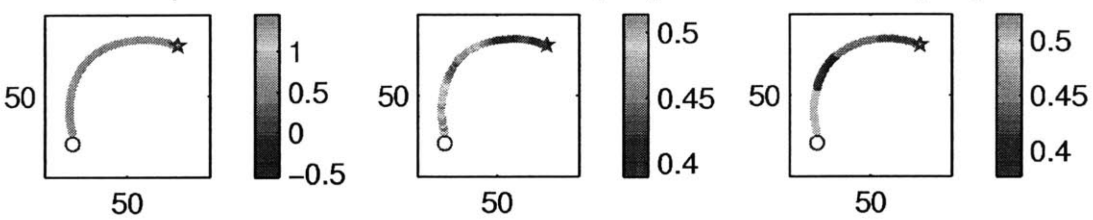

Figure 6-11: Paths for circular flow

6.4 Validation of stochastic DO-level set optimization

We validate the results from our stochastic DO level-set simulation by comparing them with the results of a direct Monte Carlo Simulation. For this purpose we choose a few realizations from the stochastic DO level-set simulation results and compare them with the numerical level-set evolution computed using a deterministic run. The aim of using the new DO level set equations is to be able to perform stochastic simulation in a computationally efficient fashion. However, we employ the deterministic Monte Carlo simulation as the ground truth for level set evolution, and hence provide a benchmark to test the level sets obtained from solving the new DO level set equations. Fig. 6-12 (Uniform Sampling), Fig. 6-13 (Random Walk Sampling), and Fig. 6-14 (Switch Sampling) shows the comparison of level set evolution for arbitrary realizations by Monte Carlo Simulation and by DO simulation. We see that the zero level sets are almost identical. We measure the discrete Frechet distance (Alt and Godau, 1995) which takes into account the location and ordering of points (Danziger, 2011), as a fraction of the grid spacing. This quantifies the measure of closeness of the zero level set contour obtained from the stochastic DO level set simulation and Monte Carlo simulation. We see that the zero level sets are different by a Frechet Distance of only of the order of grid spacing, which means that the numerical stochastic DO level-set solution introduces an error of about 1% of the domain size chosen for this illustration.

6.4.1 Comparison of DO-MC Gamma, DO-KL Gamma, and DO-Taylor Gamma with Monte Carlo

The three different methods for stochastic simulation for exploring energy utilization by vehicles are compared in this section. The circular flow is chosen for comparison. The difference in zero level set contours of fastest realization for DO-MC Gamma with Monte Carlo is shown in Fig. 6-15, for DO-KL Gamma is shown in Fig. 6-16 and

DO-Taylor Gamma is shown in Fig. 6-17. The methods perform well for the circular flow.

6.5 Conclusion

In this chapter we presented energy optimal path planning results for simple yet illustrative and important canonical flows that simulate a steady front and a steady eddy. We also demonstrated the algorithm through an illustrative example and established an analytical solution for the simulated front. In the next chapter we apply our methodology to path planning in an idealized and real ocean example.

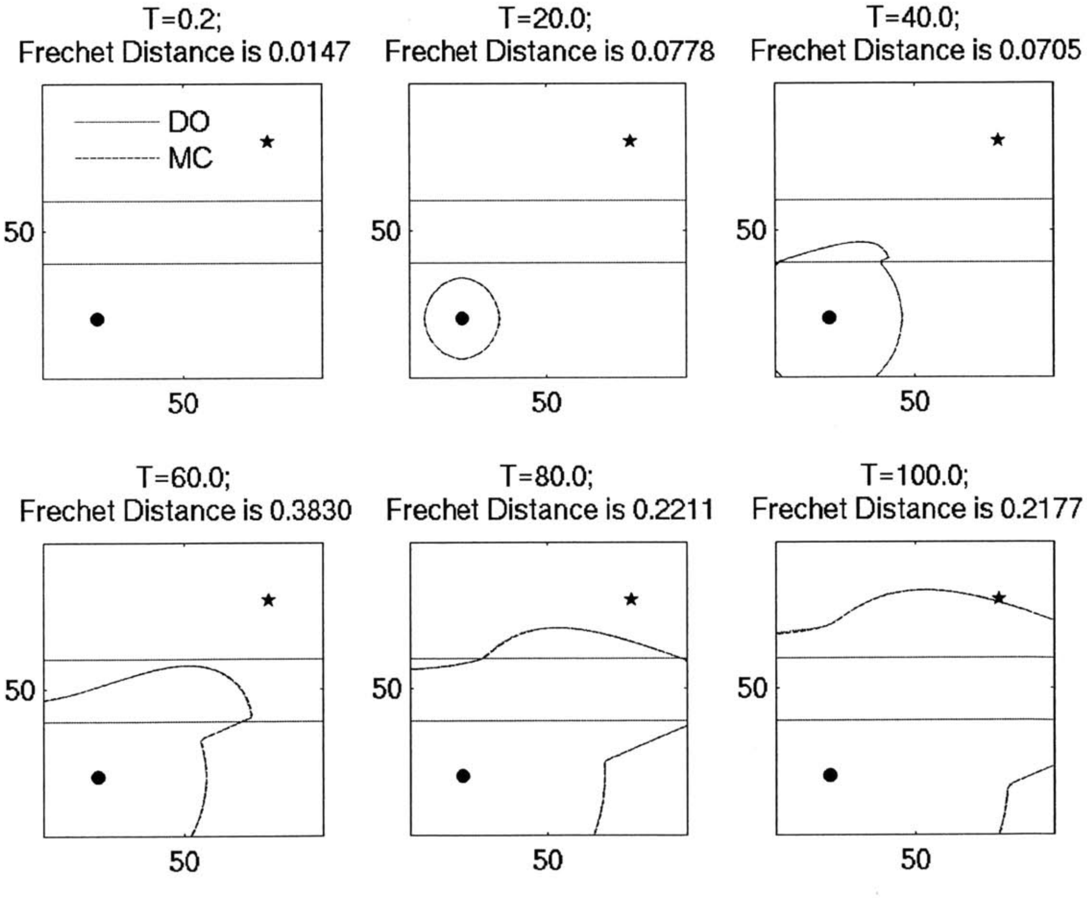

Figure 6-12: Comparing the level set evolution by the stochastic DO level set equations and by the deterministic Monte Carlo level set equation for a sample with uniform F(t) sampling strategy

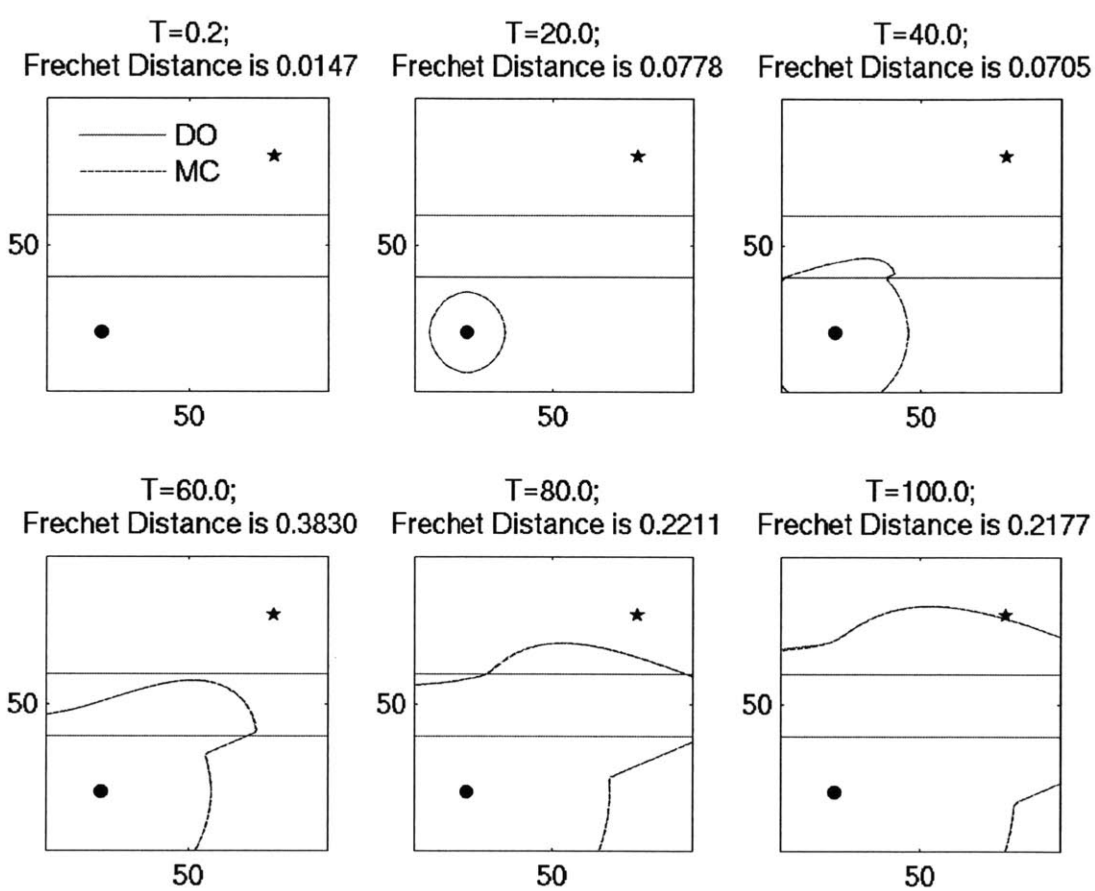

Figure 6-13: Comparing the level set evolution by the stochastic DO level set equations and by the deterministic Monte Carlo level set equation for a sample with random walk F(t) sampling strategy

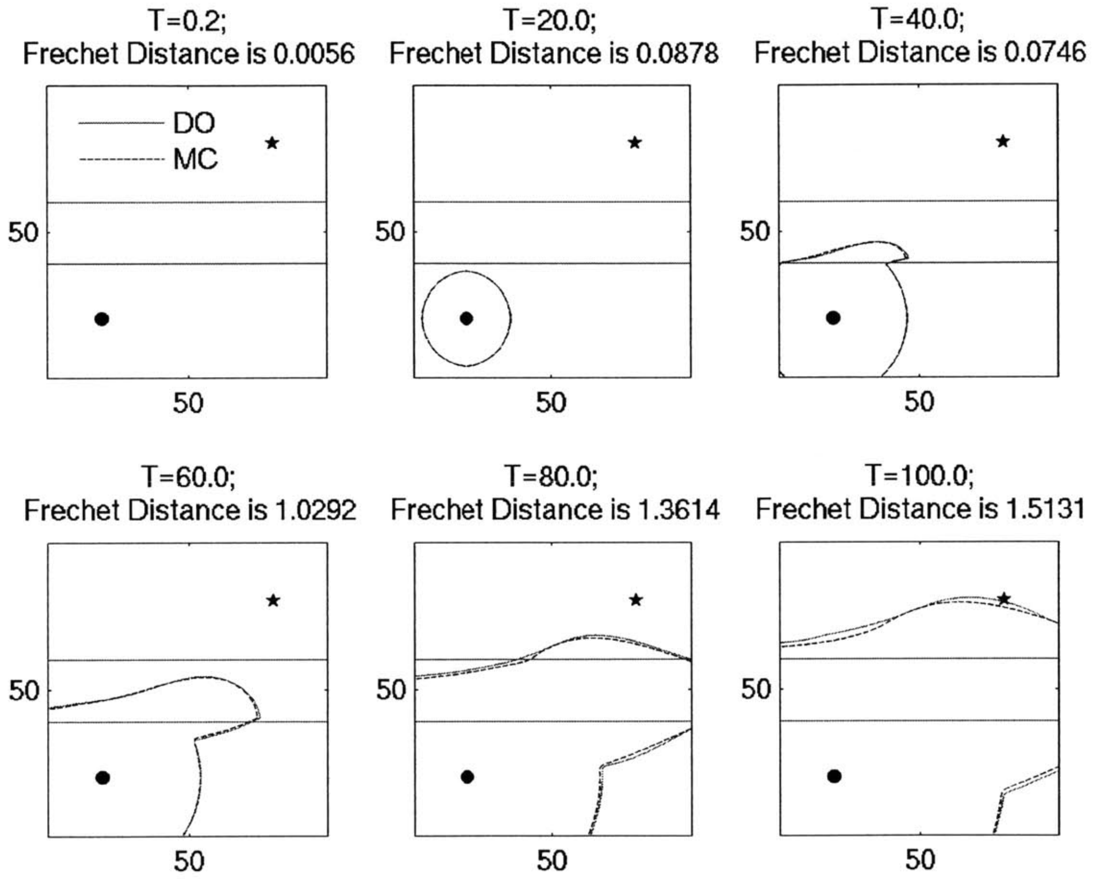

Figure 6-14: Comparing the level set evolution by the stochastic DO level set equations and by the deterministic Monte Carlo level set equation for a sample with switch sample F(t) sampling strategy

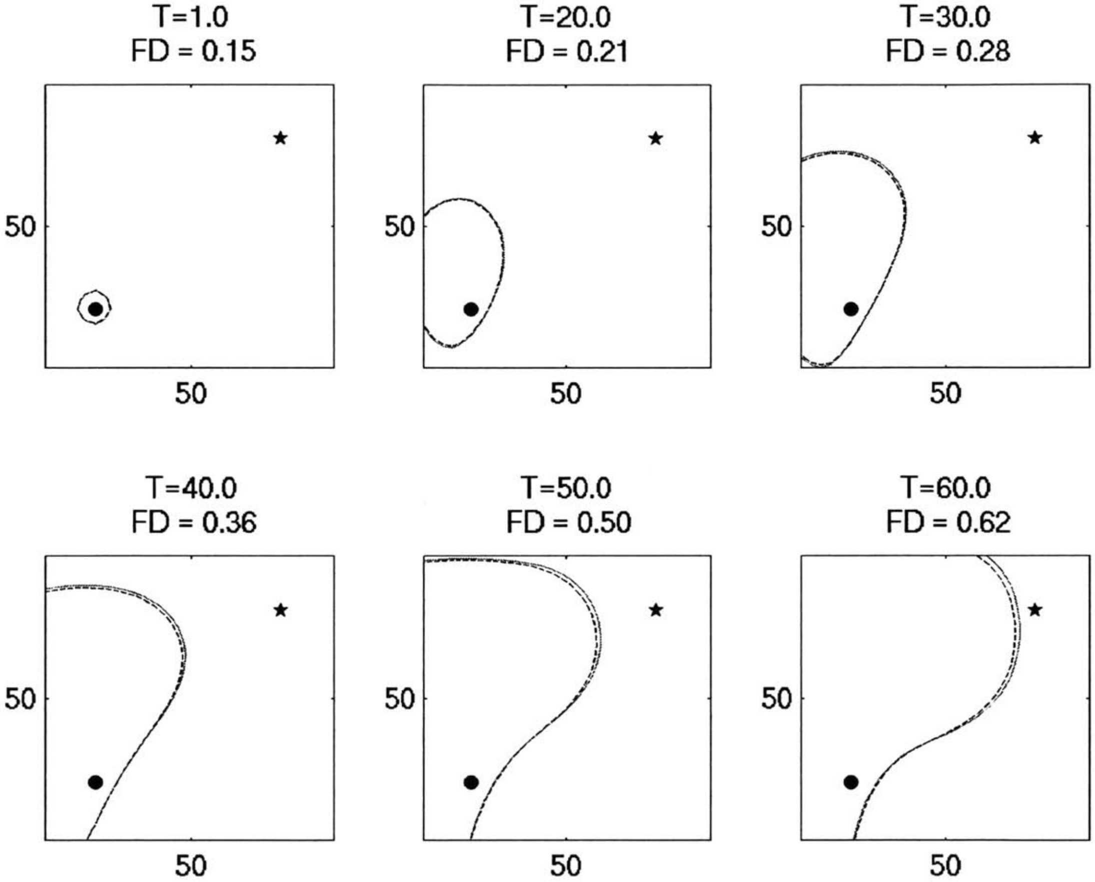

Figure 6-15: The zero level set contours obtained from DO-MC Gamma and deterministic Monte Carlo simulation are compared using Frechet Distance as a fraction of grid spacing. The contour in red is from Monte Carlo simulation and contour in black is from DO-MC simulation

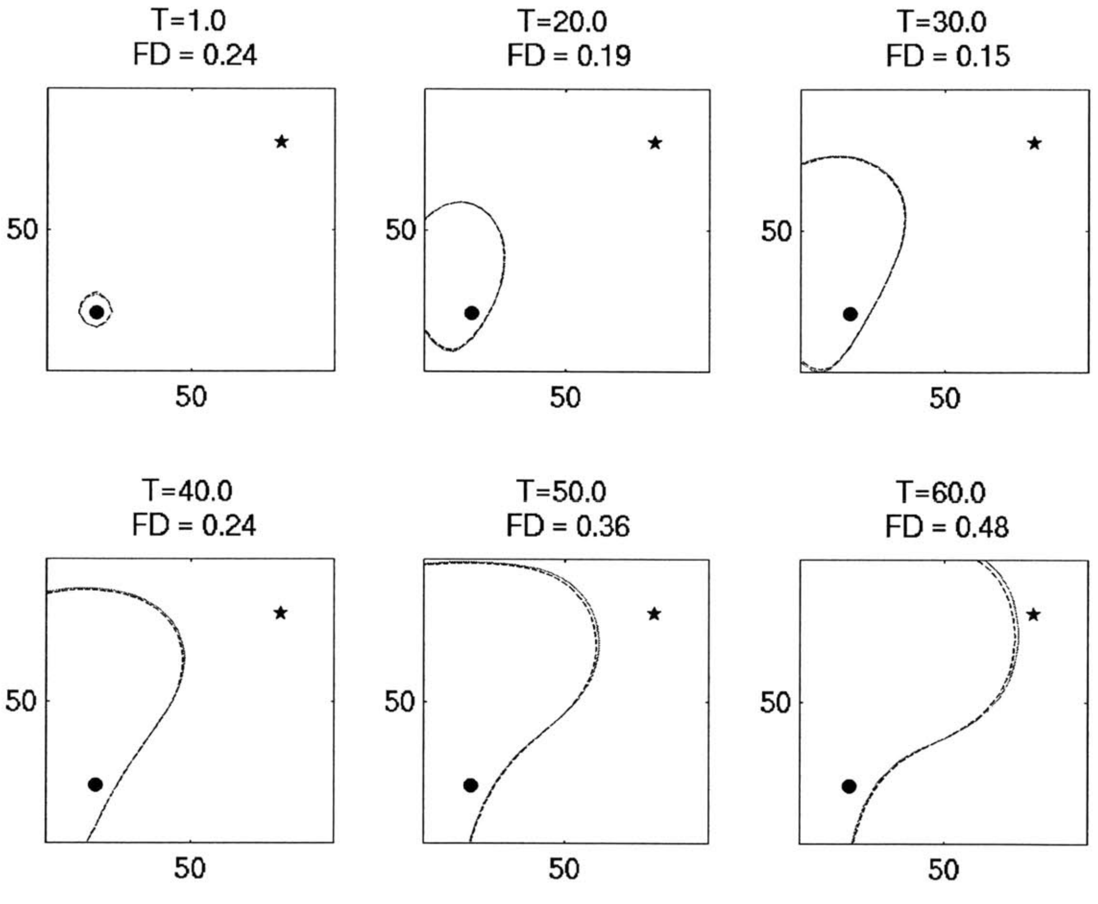

Figure 6-16: The zero level set contours obtained from DO-MC Gamma and deterministic Monte Carlo simulation are compared using Frechet Distance as a fraction of grid spacing. The contour in red is from Monte Carlo simulation and contour in black is from DO-KL Gamma simulation

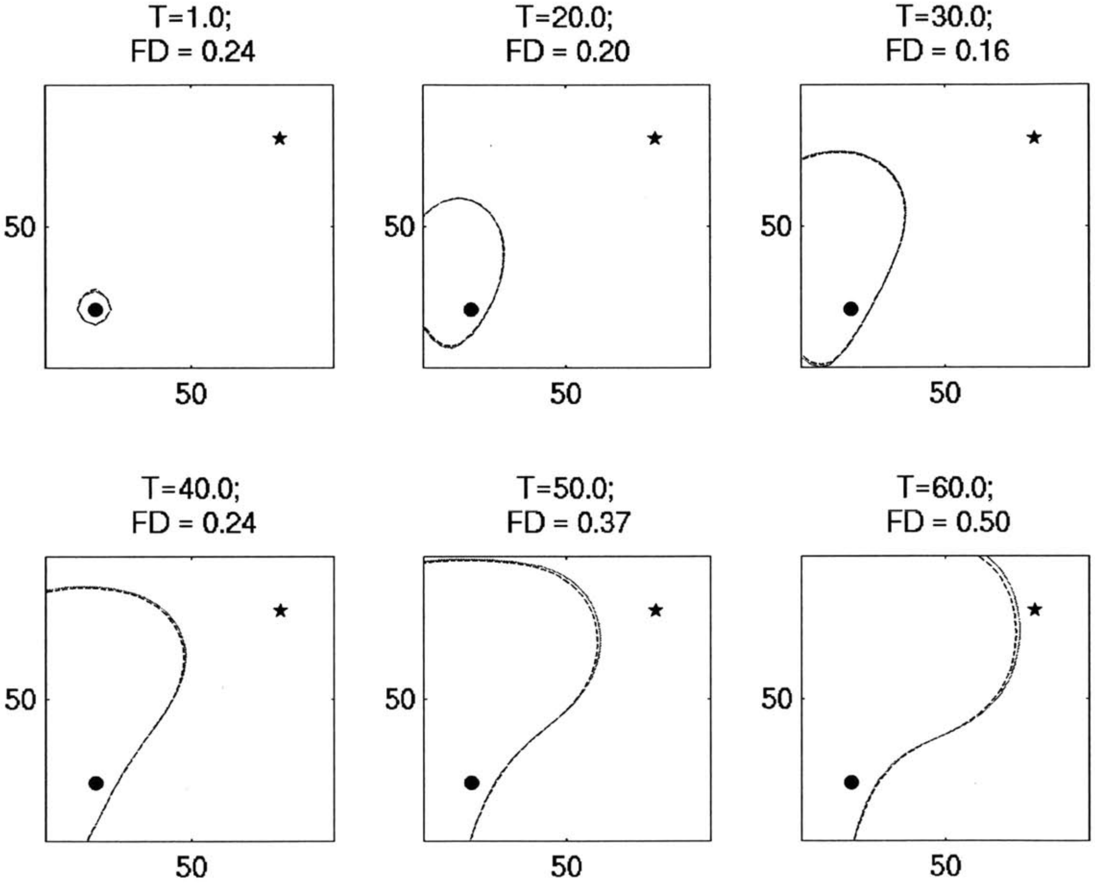

Figure 6-17: The zero level set contours obtained from DO-MC Gamma and deterministic Monte Carlo simulation are compared using Frechet Distance as a fraction of grid spacing. The contour in red is from Monte Carlo simulation and contour in black is from DO-Taylor Gamma simulation

Chapter 7

Applications: Idealized and Realistic Ocean Simulation

7.1 Introduction

In the previous chapter we applied our methodology to canonical steady flows. In the present chapter, first we apply our methodology to an idealized ocean simulation using a Double Gyre flow and study results for energy optimal path planning for different arrival times. Next we apply our methodology to a data-driven realistic ocean simulation using flow data from the MSEAS Primitive Equation model and present results for energy optimal path planning for a glider mission.

7.2 Idealized Ocean Simulation

In this section we present results from applying our stochastic DO level-set optimization methodology to a double gyre flow. A dynamic double gyre is an idealized simulation of a wind driven flow corresponding to the Jet Stream in the Atlantic and the Kuroshio in the Pacific. First we briefly outline the double gyre model, next we present the results from energy optimal path planning using new stochastic DO level-set equations.

7.2.1 Double Gyre

The wind-driven double-gyre flow is modeled using a barotropic single layer-model in a square basin of size $L = 1$ described in detail in (Dijkstra and Katsman, 1997; Simmonet et al., 2009) (see also (Pedlosky, 1998),(Cushman-Roisin and Beckers, 2010)). The intent is to simulate the idealized near-surface double-gyre ocean circulation at mid-latitudes. The mid-latitude easterlies and trade winds in the northern hemisphere drive a cyclonic gyre and an anticyclonic gyre, and the corresponding zonal jet in between. This eastward jet would correspond to the Gulf Stream in the Atlantic and to the Kuroshio and its extension in the Pacific. This idealized flow is modeled by the non-dimensional equations of motion

$$\frac{\partial u}{\partial t} = -\frac{\partial p}{\partial x} + \frac{1}{\mathrm{Re}}\Delta u - \frac{\partial (u^2)}{\partial x} - \frac{\partial (uv)}{\partial y} + fv + a\tau_x, \tag{7.1a}$$

$$\frac{\partial v}{\partial t} = -\frac{\partial p}{\partial y} + \frac{1}{\mathrm{Re}}\Delta v - \frac{\partial (vu)}{\partial x} - \frac{\partial (v^2)}{\partial y} - fu + a\tau_y, \tag{7.1b}$$

$$0 = \frac{\partial u}{\partial x} + \frac{\partial v}{\partial y}, \tag{7.1c}$$

where Re is the flow Reynolds number taking values from 10 to 10^4, $f = \tilde{f} + \beta y$ the non-dimensional Coriolis coefficient, and $a = 10^3$ the strength of the wind stress. In non-dimensional terms, we use $\tilde{f} = 0$, $\beta = 10^3$. The flow in the basin is forced by an idealized steady zonal wind stress, $\tau_x = -\frac{1}{2\pi}\cos 2\pi y$ and $\tau_y = 0$. Such dynamics was also employed for evaluating time-optimal paths by Lolla et al. (2014d).

Free slip boundary conditions are imposed on the northern and southern walls ($y = 0, 1$) and no-slip boundary conditions on the eastern and western walls ($x = 0, 1$). A 64 × 64 grid and a non-dimensional time step of 10^{-4} are used to solve both (7.1) (generation of flow-field) and stochastic DO level-set equations (4.1). The non-dimensional parameters are listed in Table [7.1] and dimensional parameters in Table [7.2]. In what follows, we present results for Re = 1000. The double gyre flow field is plotted for different times during the simulation on Fig. 7-1.

Table 7.1: Non-Dimensional Parameter list for Double Gyre simulation

Non-Dimensional Parameter	Value
$Re = \frac{UL}{A_H}$	$Re = 1000$
$a = \frac{\tau_0 L}{\rho D U^2}$	$a = 1000$
$\beta = \frac{\beta_0 L^2}{U}$	$\beta = 1000$
$f = \bar{f} + \beta y$	$\bar{f} = 0.1$

Table 7.2: Dimensional Parameter list for Double Gyre simulation

Dimensional Parameter	Value
L	10^6
D	1000
U	0.0198
A_H	19.77
β_0	1.977e-11
T	1.6 yrs

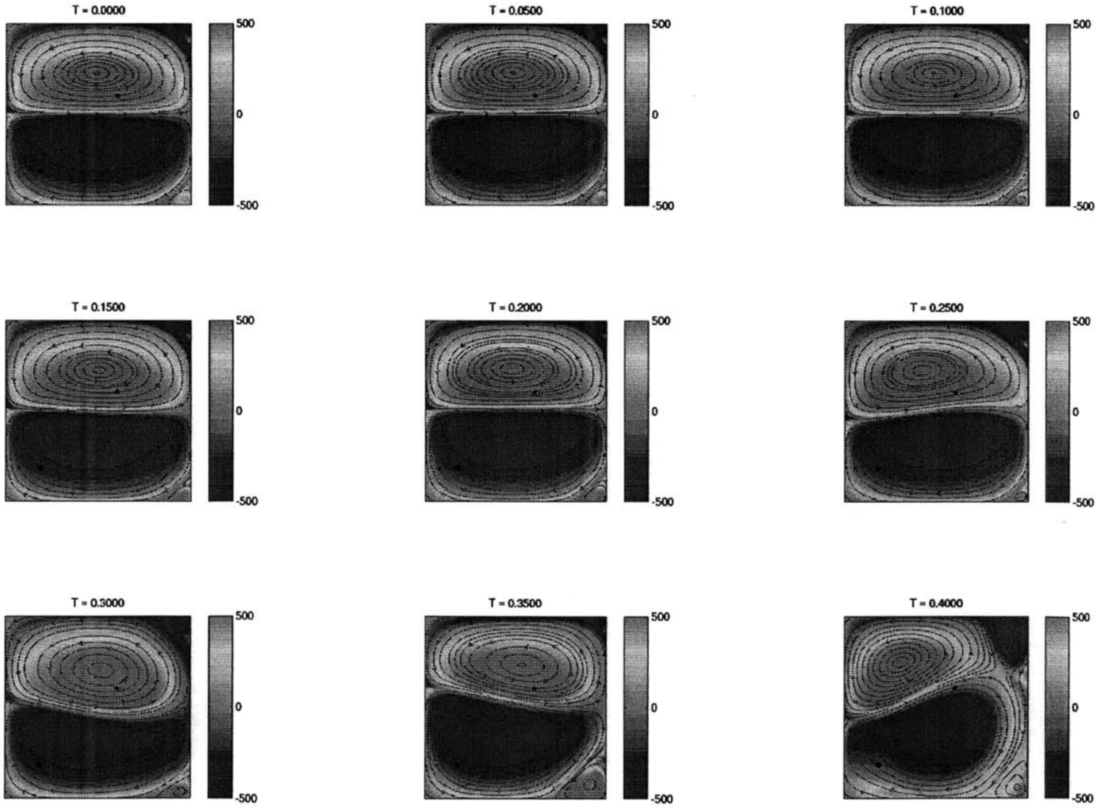
T = 0.0000

T = 0.0500

T = 0.1000

T = 0.1500

T = 0.2000

T = 0.2500

T = 0.3000

T = 0.3500

T = 0.4000

Figure 7-1: Double Gyre Flow field used in the simulation for Energy Optimal Path Planning. The figure shows snapshots at various times during the simulation.

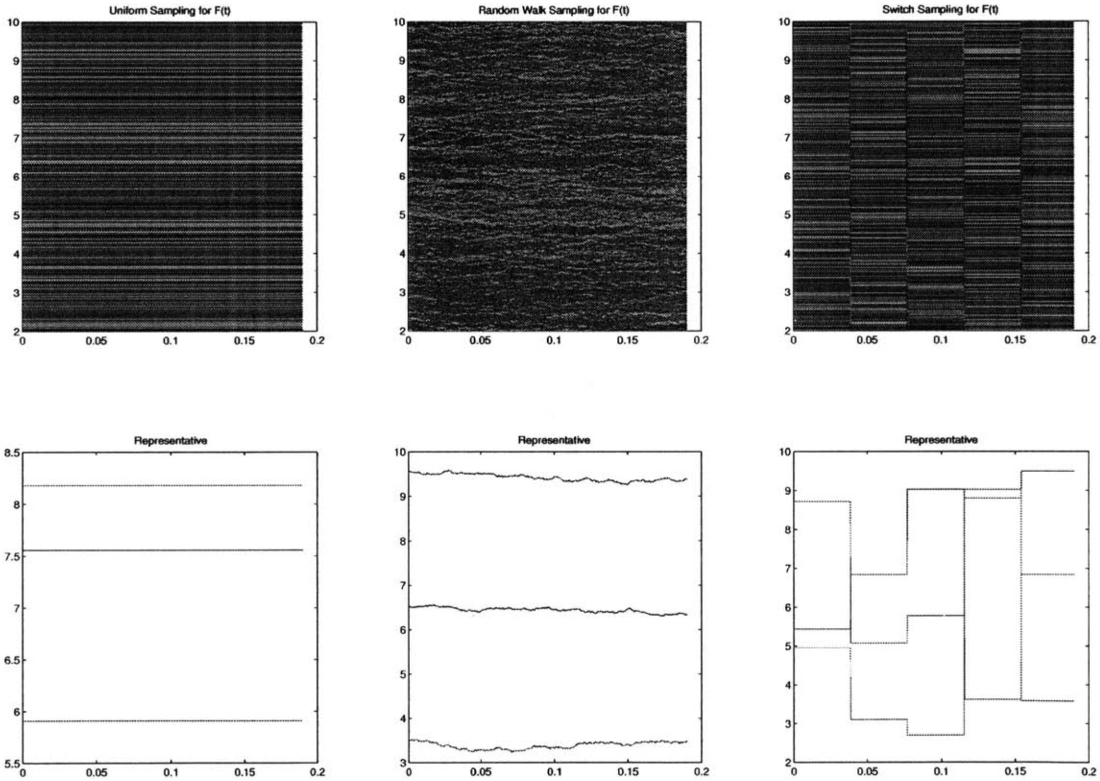

Figure 7-2: The class within which $F_{\text{DO}}(t;r)$ is sampled for energy optimal path planning in a double gyre flow

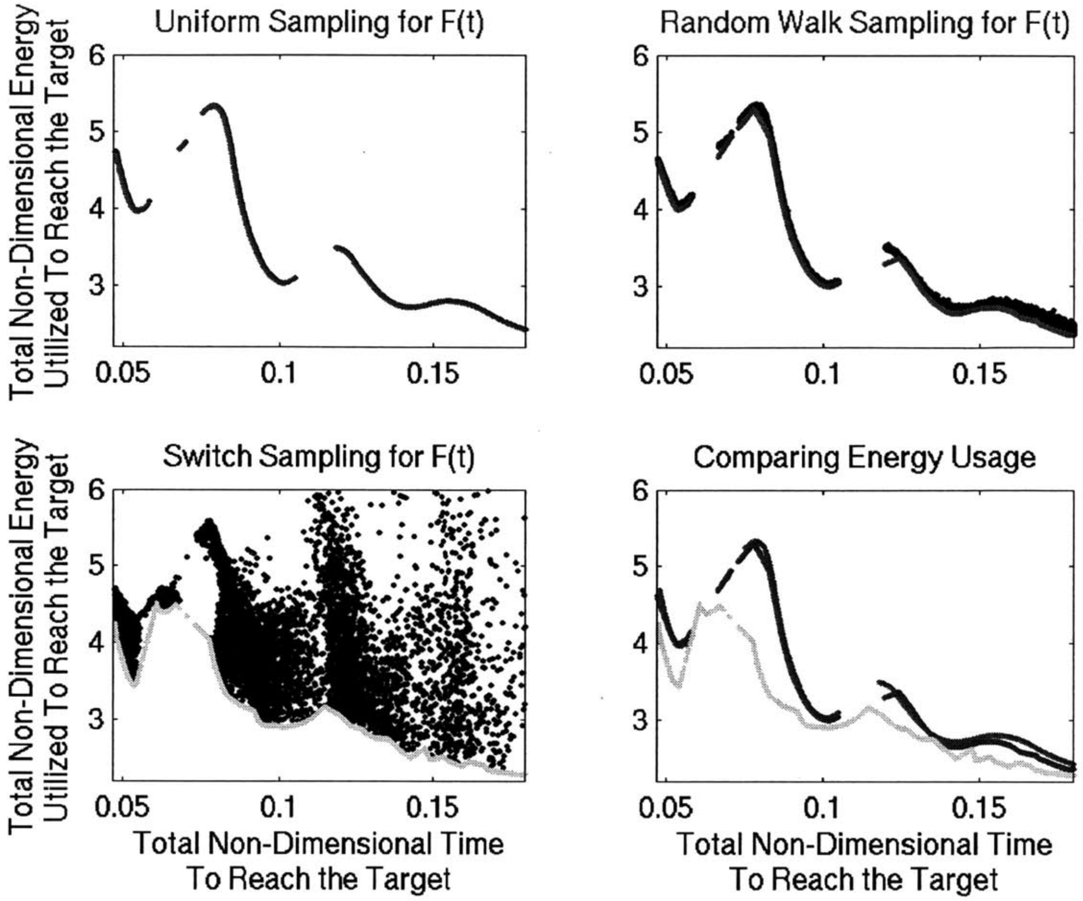

Figure 7-3: Exploring the energy utilized by a vehicle in traveling from start point (0.2,0.2) to reach a target at (0.6,0.6). The time to reach the target is obtained from our new stochastic DO level-set equations.

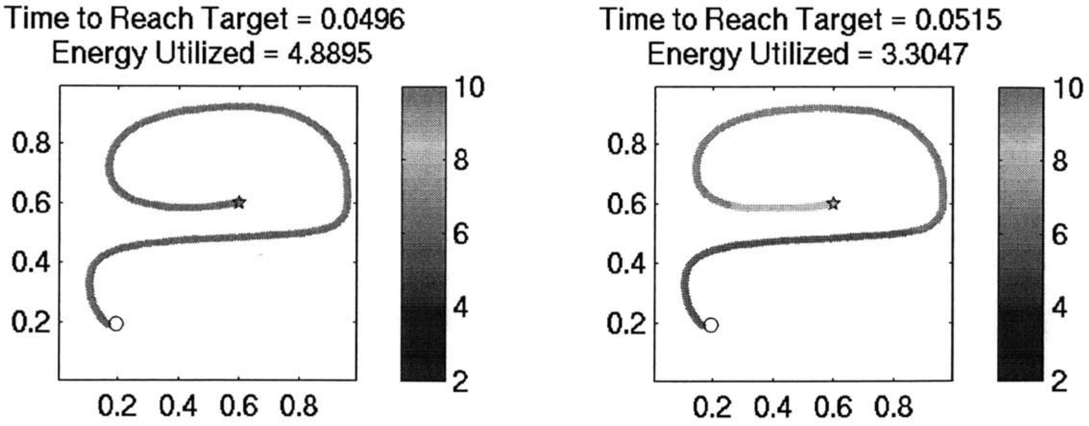

Figure 7-4: Two paths that reach between T=0.049 and T=0.052 but the path shown in right panel uses 32% less energy than path shown in left panel

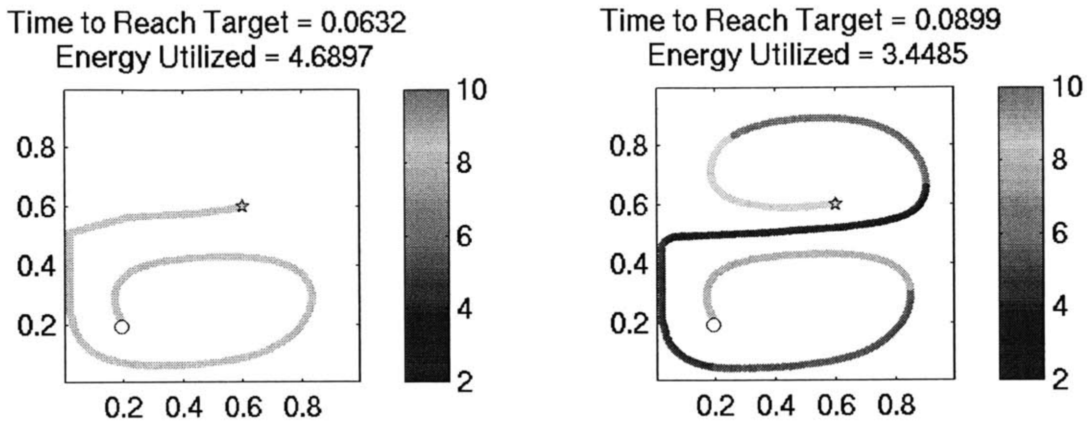
Time to Reach Target = 0.0632
Energy Utilized = 4.6897

Time to Reach Target = 0.0899
Energy Utilized = 3.4485

Figure 7-5: Two paths that reach between 0.06 and 0.09. The path on right panel, which uses a variable speed, is able to save energy

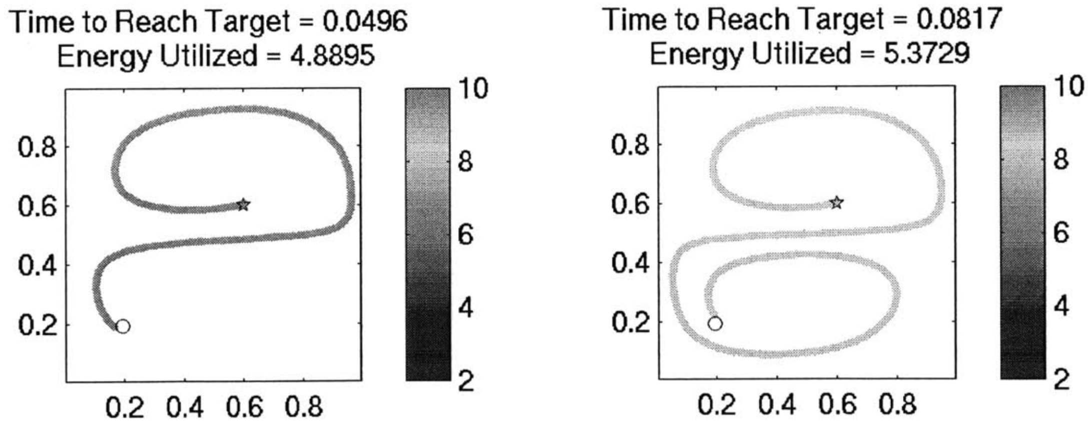
Time to Reach Target = 0.0496
Energy Utilized = 4.8895

Time to Reach Target = 0.0817
Energy Utilized = 5.3729

Figure 7-6: Two paths that use constant engine speeds. The path on the right, even though it uses the lower engine speed, takes much more time to reach and thus uses more energy.

7.2.2 Energy Path Planning in a Double Gyre Flow Field

$F_{DO}(t;r)$ is sampled from a uniform distribution, a random walk distribution and a switch sampling distribution, as shown in Fig. 7-2. The vehicle starts from the point (0.2,0.2) and the target is the point (0.6,0.6). The output of the stochastic DO level set simulation is used to explore the energy usage for different times to reach and illustrated in Fig. 7-3. Some of the paths obtained are shown in Fig. 7-4 to Fig. 7-6.

7.3 Realistic Data-driven Ocean Simulation

In this section we explore the application of our method and algorithms to a realistic ocean simulation. The mission is to start from Buzzards Bay near the Woods Hole Oceanographic Institution (WHOI) and reach a target in the Autonomous Wide Aperture Cluster for Surveillance (AWACS) region. The flow data is obtained from the data-assimilative MSEAS Primitive Equation Model. The domain is shown in Fig. 7-7. Vehicles (gliders) that travel at velocities between 10 cm/s and 30 cm/s are released from Buzzard's bay offshore from WHOI on Aug 28, 00 UTC.

7.3.1 Data-assimilative primitive-equation ocean simulations

The new stochastic DO level set equation contains a term for the advection by ocean currents. Hence, an estimate of the evolution of these currents encountered at the vehicle position is needed. The currents are here obtained from a MSEAS multiresolution two-way nested tidally-driven primitive-equation simulation (Haley and Lermusiaux, 2010). Specifically, they are produced from a reanalysis of the real-time AWACS and SW06 exercises (Aug.-Sep. 2006) in the New Jersey Shelf/Hudson Canyon region (WHOI, 2006; Lermusiaux et al., 2006; Chapman and Lynch, 2010; Lin et al., 2010). This reanalysis is a free surface simulation employing two-way implicit nesting with tidal (Egbert and Erofeeva, 2002; Logutov and Lermusiaux, 2008) and atmospheric (WRF/NOGAPS) forcing, covering the period 14 Aug - 24 Sep 2006. Details of the discretization and model numerics are given in Haley and Lermusiaux (2010). In situ

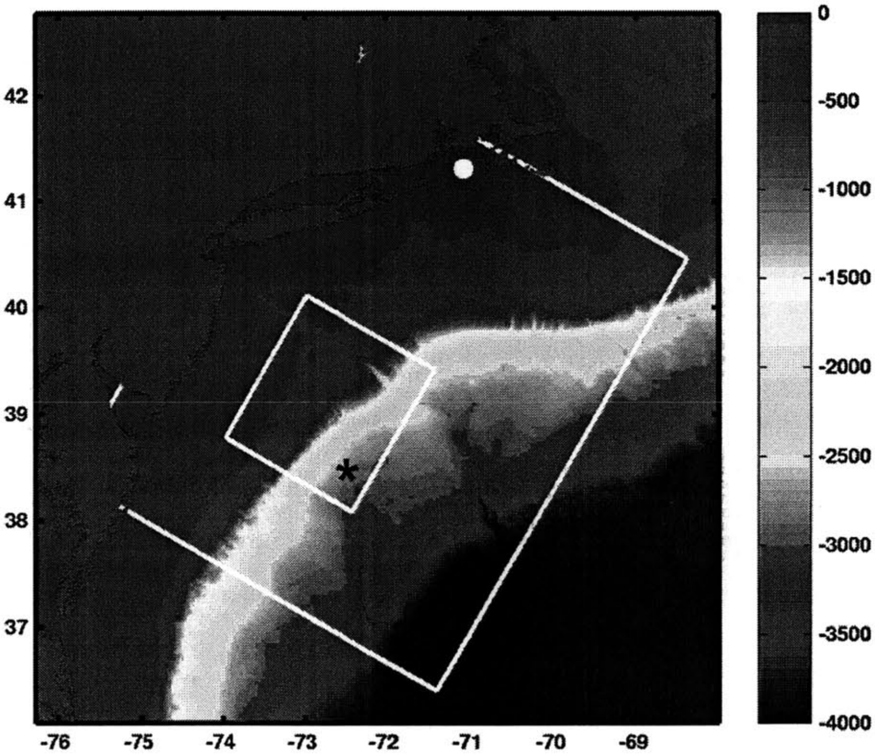
42
41
40
39
38
37
-76
-75
-74
-73
-72
-71
-70
-69
0
-500
-1000
-1500
-2000
-2500
-3000
-3500
-4000

Figure 7-7: The start point is marked as a circle and the end point is marked as a star. The color axis shows the depth.

observations from Rutgers SeaGliders, NMFS cruises, CTD casts collected aboard the research vessels Knorr, Quest and Tioga, as well as Scanfish data are used to create the initial conditions and for assimilation. SST is also assimilated on Aug 14, 17, 19, 21, 23, 25. Additional synoptic data (WODB, GTSPP) and pseudo profiles were incorporated to bolster the shelf-break front. A temperature/salinity based feature model representation of the Gulf Stream was included off shore.

For the present application, we assume that all gliders follow the same yo-yo pattern in the vertical and that the ocean vertical velocities are small and accounted for in the forward motions of vehicles. With these assumptions, what differentiates the vehicles is then simply their nominal forward horizontal speeds in these yo-yo vertical-horizontal motions. We consider yo-yo patterns from the near surface to either the local near bottom or 400 m depth, whichever is shallower (for the mission considered, a large portion of the path occurs on the shelf, within 0 to 100m or less). We assume that the time scales of the horizontal currents variability are not much shorter than the time to complete a single vertical excursion (which is acceptable in shallower water, even in the presence of tidal currents). Within our assumptions, the horizontal currents that a vehicle would actually encounter during its yo-yo motion would be the horizontal currents integrated along its path, from the near surface to either the local near bottom or 400 m depth. Of course, it is the path of the vehicle that determines which currents are actually encountered, hence the need for our energy-optimal path planning.

7.3.2 Energy Optimal Path Planning for Mission

The new stochastic DO level-set based energy optimal path planning optimization is applied to the problem. Level sets and paths for fastest and slowest vehicles are shown in Fig. 7-8. All other vehicles will take an intermediate time between these the corresponding two times, with different level set evolutions and paths. The energy utilized by different engine speed time history is explored in Fig. 7-9. The optimization is then performed to identify samples of engine speed time-history which are optimal for the given class of $F_{DO}(t;r)$ samples. The energy-optimal paths are then obtained

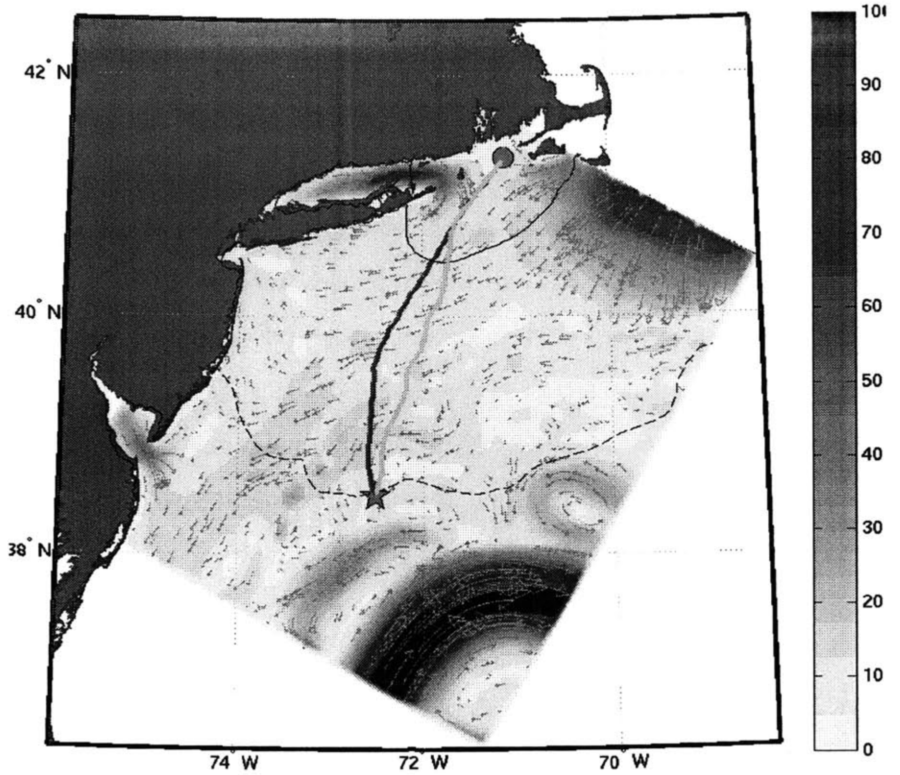

Figure 7-8: The red path is the path for a vehicle with F_{max} and the green path is for the vehicle with F_{min}. The level set contours for the both vehicles at the time at which the faster vehicle reaches the target is shown in black, overlaid on ocean currents at that time

by back tracking and shown in Fig. 7-10 and Fig. 7-11

7.4 Conclusion

In this chapter we showed the application of our methodology to an idealized ocean simulation using a Double Gyre flow and in a realistic data-assimilative ocean simulation for a mission performed from WHOI to the New Jersey shelf/Hudson Canyon region.

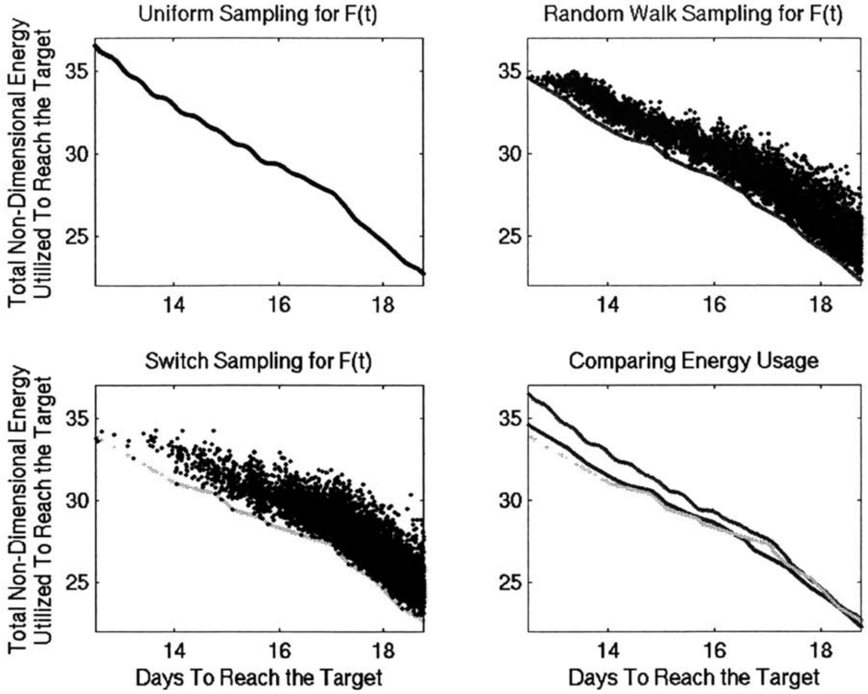

Figure 7-9: The stochastic DO level-set simulations are used to explore different energy utilizations for Glider mission durations of 19 days and under, aiming to find sets of optimal energy paths within that a pre-selected stochastic class of vehicle speed time-history.

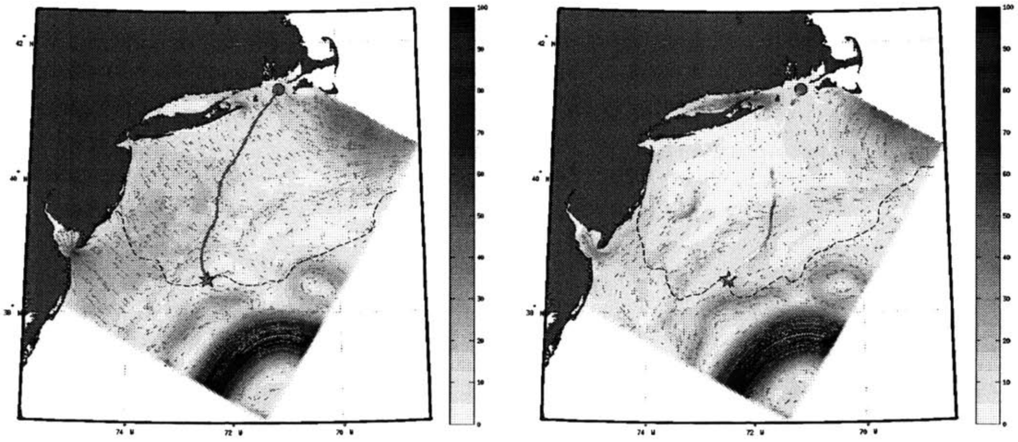

(a) (b)

Figure 7-10: (a) is a path that reaches in the shortest time, 12.96 days, but consuming highest energy and (b) shows a path that takes 6 days more to complete the mission (18.78 days in total), but utilizes 40% lower energy. The vehicle speed along the path is plotted in color

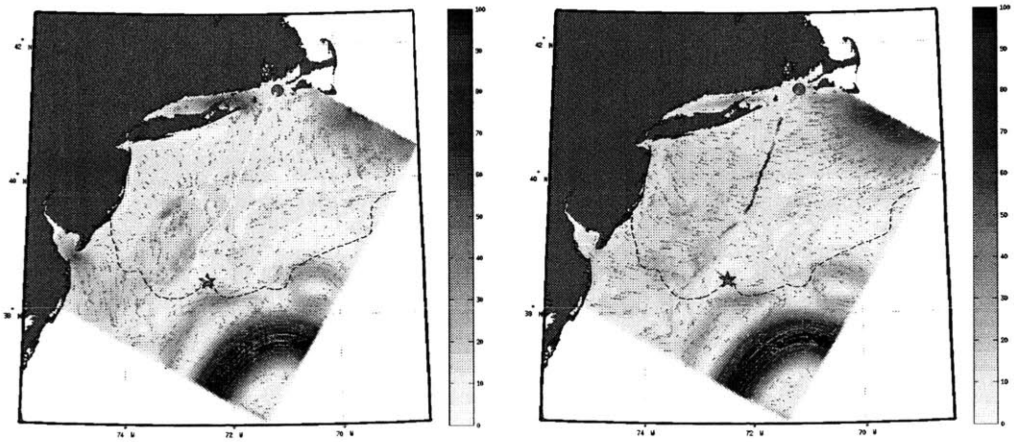
(a) (b)

Figure 7-11: (a) is a path that reaches in 16 days using a constant speed and (b) shows a path that takes 16 days but has an engine speed obtained from switch sampling, and this utilizes lower energy (about 10% lower) than the path which uses constant speed

Chapter 8

Conclusion and Future Work

In this thesis we developed new stochastic Dynamically Orthogonal Level Set Equations for computing energy optimal paths among all time optimal paths. A rigorous theory was presented to obtain optimal paths within chosen stochastic classes of nominal speeds $F(t, \omega)$. The method developed here is valid for any flows (strong, time-dependent or not). The computational advantage arises from the utilization of the nonlinearities of the environment for efficient DO reduction of the large time-increasing dimensionality of the stochastic optimization. As the DO coefficients are presently integrated by a Monte-Carlo (MC) approach, it allows fast selection/sort of minimum energy paths during the optimization phase of the algorithm.

The schemes and implementation was verified by extensive studies. For treating the non-polynomial non-linearity, a diagnostic update scheme was proposed and three methods for evaluating the non-polynomial non-linearity were developed and evaluated. Results on varied test cases of increasing complexities indicate that the scheme is usable to guide real vehicles in realistic ocean applications. There are interesting possibilities for the approach and software developed, from national labs and industry, in part because of the wide range of applications and needs (ocean, air, land).

In the future, energy-optimal path planning can be extended to apply in cases with multiple end-points, for coordinated vehicles, and in uncertain flow predictions. For example, DO level set methods can be extended to handle multi-modal distributions of level sets. In addition, realistic Bayesian Nonlinear Assimilation and Path

Planning can be combined to develop and apply schemes and computational systems for rigorous Bayesian assimilation of Eulerian and Lagrangian coastal flow data, exploiting the nonlinearities of the governing equations and the mutual information structures inherent to 4D coastal ocean dynamics. These schemes can then be applied for coordinated energy-time-optimal path planning in realistic coastal applications.

Bibliography

Aghababa, M. P. (2012). 3d path planning for underwater vehicles using five evolutionary optimization algorithms avoiding static and energetic obstacles. *Applied Ocean Research*, 38:48–62.

Alt, H. and Godau, M. (1995). Computing the fréchet distance between two polygonal curves. *International Journal of Computational Geometry & Applications*, 5(01n02):75–91.

Alvarez, A., Caiti, A., and Onken, R. (2004). Evolutionary path planning for autonomous underwater vehicles in a variable ocean. *IEEE Journal of Oceanic Engineering*, 29(2):418–429.

Athans, M. and Falb, P. (2006). *Optimal Control: An Introduction to the Theory And Its Applications.* Dover Books on Engineering Series. Dover Publications.

Bachmayer, R., Leonard, N. E., Graver, J., Fiorelli, E., Bhatta, P., and Paley, D. (2004). Underwater gliders: Recent developments and future applications. In *in Proc. IEEE International Symposium on Underwater Technology (UTÂŠ04*.

Bahr, A., Leonard, J. J., and Fallon, M. F. (2009). Cooperative localization for autonomous underwater vehicles. *The International Journal of Robotics Research*, 28(6):714–728.

Barraquand, J., Langlois, B., and Latombe, J. C. (1992). Numerical potential field techniques for robot path planning. *IEEE Transactions on Systems, Man, and Cybernetics*, 22(2):224–241.

Bellingham, J. G. and Rajan, K. (2007). Robotics in remote and hostile environments. *Science*, 318(5853):1098–1102.

Beylkin, D. (2008). Path optimization for an earth-based demonstration balloon flight.

Bhatta, P., Fiorelli, E., Lekien, F., Leonard, N. E., Paley, D. A., Zhang, F., Bachmayer, R., Davis, R. E., Fratantoni, D. M., and Sepulchre, R. (2005). Coordination of an underwater glider fleet for adaptive sampling. In *in Proceedings of International Workshop on Underwater Robotics*, pages 61–69.

Bruce, J. and Veloso, M. (2002). Real-time randomized path planning for robot navigation. In *Proceedings of IROS-2002*, Switzerland.

Bryson, A. E. and Ho, Y. C. (1975). *Applied Optimal Control: Optimization, Estimation and Control.* John Wiley and Sons.

Carroll, K., McClaran, S., Nelson, E., Barnett, D., Friesen, D., and William, G. (1992). AUV path planning: An A* approach to path planning with consideration of variable vehicle speeds and multiple, overlapping, time-dependent exclusion zones. In *Proceedings of the Symposium on Autonomous Underwater Vehicle Technology*, pages 79–84.

Chakrabarty, A. and Langelaan, J. (2013). Uav flight path planning in time varying complex wind-fields. In *American Control Conference (ACC), 2013*, pages 2568–2574. IEEE.

Chapman, N. R. and Lynch, J. F. (2010). Special issue on the 2006 shallow water experiment. *IEEE Journal of Oceanic Engineering*, 35(1):1–2.

Chien-Chou, S., Yih, Y., Mong-Fong, H., Tien-Szu, P., and Jeng-Shyang, P. (2014). A framework to evolutionary path planning for autonomous underwater glider. In Ali, M., Pan, J.-S., Chen, S.-M., and Horng, M.-F., editors, *Modern Advances in Applied Intelligence*, volume 8482 of *Lecture Notes in Computer Science*, pages 1–11. Springer International Publishing.

Curtin, T. B. and Bellingham, J. G. (2009). Progress toward autonomous ocean sampling networks. *Deep Sea Research Part II: Topical Studies in Oceanography*, 56(3):62–67.

Cushman-Roisin, B. and Beckers, J. (2010). *Introduction to Geophysical Fluid Dynamics. Physical and Numerical aspects.* Academic Press.

Danziger, Z. (2011). MATLAB code for calculating discrete frechet distance. `http://www.mathworks.com/matlabcentral/fileexchange/31922-discrete-frechet-distance`. [Online; accessed 8-Aug-2014].

Debusschere, B. J., Najm, H. N., Pébay, P. P., Knio, O. M., Ghanem, R. G., and Maître, O. P. L. (2005). Numerical challenges in the use of polynomial chaos representations for stochastic processes. *SIAM Journal on Scientific Computing*, 26(2):698–719.

Dijkstra, H. and Katsman, C. (1997). Temporal variability of the wind-driven quasi-geostrophic double gyre ocean circulation: Basic bifurcation diagrams. *Geophysics Astrophysics Fluid Dynamics*, 85:195–232.

Egbert, G. D. and Erofeeva, S. Y. (2002). Efficient inverse modeling of barotropic ocean tides. *Journal of Atmospheric and Oceanic Technology*, 19(2):183–204.

Elisseeff, P., Schmidt, H., Johnson, M., Herold, D., Chapman, N. R., and McDonald, M. M. (1999). Acoustic tomography of a coastal front in Haro Strait, British Columbia. *The Journal of the Acoustical Society of America*, 106(1):169–184.

Eriksen, C. C., Osse, T. J., Light, R. D., Wen, T., Lehman, T. W., Sabin, P. L., Ballard, J. W., and Chiodi, A. M. (2001). Seaglider: A long-range autonomous underwater vehicle for oceanographic research. *Oceanic Engineering, IEEE Journal of*, 26(4):424–436.

Garau, B., Bonet, M., Alvarez, A., Ruiz, S., and Pascual, A. (2009a). Path planning for autonomous underwater vehicles in realistic oceanic current fields: Application to gliders in the Western Mediterranean Sea. *Journal of Maritime Research*, 6(2):5–22.

Garau, B., Bonet, M., Alvarez, A., Ruiz, S., Pascual, A., et al. (2009b). Path planning for autonomous underwater vehicles in realistic oceanic current fields: Application to gliders in the western mediterranean sea. *Journal of Maritime Research*, 6(2):5–22.

Gugercin, S. (2005). An iterative svd-krylov based method for model reduction of large-scale dynamical systems. In *Decision and Control, 2005 and 2005 European Control Conference. CDC-ECC'05. 44th IEEE Conference on*, pages 5905–5910. IEEE.

Haley, Jr., P. J. and Lermusiaux, P. F. J. (2010). Multiscale two-way embedding schemes for free-surface primitive equations in the "Multidisciplinary Simulation, Estimation and Assimilation System". *Ocean Dynamics*, 60(6):1497–1537.

Hoare, C. A. (1962). Quicksort. *The Computer Journal*, 5(1):10–16.

Hsieh, M. A., Forgoston, E., Mather, T. W., and Schwartz, I. B. (2012). Robotic manifold tracking of coherent structures in flows. In *Robotics and Automation (ICRA), 2012 IEEE International Conference on*, pages 4242–4247. IEEE.

Hwang, Y. K. and Ahuja, N. (1992). Gross motion planningâĂŤa survey. *ACM Computing Surveys (CSUR)*, 24(3):219–291.

Inanc, T., Shadden, S. C., and Marsden, J. E. (2005). Optimal Trajectory Generation in Ocean Flows. In *Proceedings of American Control Conference*, volume 1, pages 674–679.

Jaillet, L., Cortés, J., and Siméon, T. (2010). Sampling-based path planning on configuration-space costmaps. *Robotics, IEEE Transactions on*, 26(4):635–646.

Julier, S. J. and Uhlmann, J. K. (1996). A general method for approximating nonlinear transformations of probability distributions. Technical report, Technical report, Robotics Research Group, Department of Engineering Science, University of Oxford.

Karaman and Frazzoli (2011). Sampling-based algorithms for optimal motion planning. *International Journal of Robotics Research*, 30(7):846–894.

Kavraki, L. E., Svestka, P., Latombe, J.-C., and Overmars, M. H. (1996). Probabilistic roadmaps for path planning in high-dimensional configuration spaces. *Robotics and Automation, IEEE Transactions on*, 12(4):566–580.

Kruger, D., Stolkin, R., Blum, A., and Briganti, J. (2007). Optimal AUV path planning for extended missions in complex, fast-flowing estuarine environments. In *Robotics and Automation, 2007 IEEE International Conference on*, pages 4265–4270.

Kuffner, J. J. and LaValle, S. M. (2000). RRT-connect: An efficient approach to single-query path planning. In *Proceedings of IEEE International Confernce on Robotics and Automation*, pages 995–1001.

Latombe, J.-C. (1996). Robot motion planning, chapter.

Lavalle, S. M. (1998). Rapidly-exploring Random Trees: A new tool for path planning. Technical report, Iowa State University.

LaValle, S. M. (2006). *Planning algorithms*. Cambridge university press.

LaValle, S. M. and Hutchinson, S. A. (1998). Optimal motion planning for multiple robots having independent goals. *Robotics and Automation, IEEE Transactions on*, 14(6):912–925.

Leonard, N. E., Paley, D. A., Davis, R. E., Fratantoni, D. M., Lekien, F., and Zhang, F. (2010). Coordinated control of an underwater glider fleet in an adaptive ocean sampling field experiment in monterey bay. *Journal of Field Robotics*, 27(6):718–740.

Lermusiaux, P. F. J., Haley, Jr., P. J., Leslie, W. G., Logoutov, O., and Robinson, A. R. (2006). Autonomous Wide Aperture Cluster for Surveillance (AWACS): Adaptive Sampling and Search Using Predictive Models with Coupled Data Assimilation and Feedback - Harvard Page.

Lermusiaux, P. F. J., Lolla, T., Haley Jr., P. J., Yigit, K., Ueckermann, M. P., Sondergaard, T., and Leslie, W. G. (2014). *Science of Autonomy: Time-Optimal Path Planning and Adaptive Sampling for Swarms of Ocean Vehicles*. Chapter 11, Springer Handbook of Ocean Engineering: Autonomous Ocean Vehicles, Subsystems and Control, Tom Curtin (Ed.). in press.

Lin, Y.-T., Newhall, A. E., Duda, T. F., Lermusiaux, P. F. J., and Haley, P. J. (2010). Merging multiple-partial-depth data time series using objective empirical orthogonal function fitting. *IEEE Journal of Oceanic Engineering*, 35(4):710–721.

Logutov, O. G. and Lermusiaux, P. F. J. (2008). Inverse barotropic tidal estimation for regional ocean applications. *Ocean Modelling*, 25(1–2):17–34.

Lolla, T. (2012). Path planning in time dependent flows using level set methods. Master's thesis, Department of Mechanical Engineering, Massachusetts Institute of Technology.

Lolla, T., Haley, P. J., and Lermusiaux, P. F. J. (2014a). Path planning in multiscale ocean flows: coordination, pattern formation and dynamic obstacles. *Ocean Modeling*. to be submitted.

Lolla, T., Haley, Jr., P. J., and Lermusiaux, P. F. J. (2014b). Time-optimal path planning in dynamic flows using level set equations: Realistic applications. *Ocean Dynamics*. In press.

Lolla, T., Lermusiaux, P. F. J., Ueckermann, M. P., and Haley, Jr., P. J. (2014c). Modified level set approaches for the planning of time-optimal paths for swarms of ocean vehicles. MSEAS Report 14, Department of Mechanical Engineering, Massachusetts Institute of Technology, Cambridge, MA, USA.

Lolla, T., Lermusiaux, P. F. J., Ueckermann, M. P., and Haley, Jr., P. J. (2014d). Time-optimal path planning in dynamic flows using level set equations: Theory and schemes. *Ocean Dynamics*. In press.

Lolla, T., Ueckermann, M. P., Yigit, K., Haley, P. J., and Lermusiaux, P. F. J. (2012). Path planning in time dependent flow fields using level set methods. In *Proceedings of IEEE International Conference on Robotics and Automation*, pages 166–173.

McKeeman, B. and Shure, L. (2004). Details of MATLAB's sort implementation. `http://www.mathworks.com/company/newsletters/articles/an-adventure-of-sortsbehind-the-scenes-of-a-matlab-upgrade.html`. [Online; accessed 3-Aug-2014].

McLain, T. W. and Beard, R. W. (1998). Successive galerkin approximations to the nonlinear optimal control of an underwater robotic vehicle. In *Robotics and Automation, 1998. Proceedings. 1998 IEEE International Conference on*, volume 1, pages 762–767. IEEE.

Melchior, N. A. and Simmons, R. (2007). Particle RRT for path planning with uncertainty. In *Robotics and Automation, 2007 IEEE International Conference on*, pages 1617–1624.

Michini, M., Hsieh, M. A., Forgoston, E., and Schwartz, I. B. (2014). Robotic tracking of coherent structures in flows.

Osher, S. and Sethian, J. A. (1988). Fronts propagating with curvature-dependent speed: Algorithms based on Hamilton-Jacobi formulations. *Journal of Computational Physics*, 79(1):12 – 49.

Pedlosky, J. (1998). *Ocean Circulation Theory*. Springer-Verlag.

Petres, C., Pailhas, Y., Patron, P., Petillot, Y., Evans, J., and Lane, D. (2007). Path planning for autonomous underwater vehicles. *Robotics, IEEE Transactions on*, 23(2):331 –341.

Ramp, S. R., Davis, R. E., Leonard, N. E., Shulman, I., Chao, Y., Robinson, A. R., Marsden, J., Lermusiaux, P. F. J., Fratantoni, D. M., Paduan, J. D., Chavez, F. P., Bahr, F. L., Liang, S., Leslie, W., and Li, Z. (2009). Preparing to predict: The second Autonomous Ocean Sampling Network (AOSN-II) experiment in the Monterey Bay. *Deep Sea Research Part II: Topical Studies in Oceanography*, 56(3–5):68–86. doi:10.1016/j.dsr2.2008.08.013.

Rao, D. and Williams, S. B. (2009). Large-scale path planning for underwater gliders in ocean currents. In *Proceedings of Australasian Conference on Robotics and Automation.*

Rudnick, D. L., Davis, R. E., Eriksen, C. C., Fratantoni, D. M., and Perry, M. J. (2004). Underwater gliders for ocean research. *Marine Technology Society Journal*, 38(2):73–84.

Sapsis, T. P. and Lermusiaux, P. F. J. (2009). Dynamically orthogonal field equations for continuous stochastic dynamical systems. *Physica D: Nonlinear Phenomena*, 238(23–24):2347–2360. doi:10.1016/j.physd.2009.09.017.

Sapsis, T. P. and Lermusiaux, P. F. J. (2012). Dynamical criteria for the evolution of the stochastic dimensionality in flows with uncertainty. *Physica D: Nonlinear Phenomena*, 241(1):60–76.

Schmidt, H., Bellingham, J. G., Johnson, M., Herold, D., Farmer, D., and Pawlowicz, R. (1996). Real-time frontal mapping with AUVs in a coastal environment. In *OCEANS '96. MTS/IEEE. Prospects for the 21st Century. Conference Proceedings*, volume 3, pages 1094 –1098.

Schofield, O., Glenn, S., Orcutt, J., Arrott, M., Meisinger, M., Gangopadhyay, A., Brown, W., Signell, R., Moline, M., Chao, Y., Chien, S., Thompson, D., Balasuriya, A., Lermusiaux, P. F. J., and Oliver, M. (2010). Automated sensor networks to advance ocean science. *Eos Trans. AGU*, 91(39):345–346.

Schofield, O., Kohut, J., Aragon, D., Creed, L., Graver, J., Haldeman, C., Kerfoot, J., Roarty, H., Jones, C., Webb, D., et al. (2007). Slocum gliders: Robust and ready. *Journal of Field Robotics*, 24(6):473–485.

Sethian, J. A. (1999a). Fast marching methods. *SIAM Rev.*, 41(2):199–235.

Sethian, J. A. (1999b). *Level Set Methods and Fast Marching Methods: Evolving Interfaces in Computational Geometry, Fluid Mechanics, Computer Vision, and Materials Science.* Cambridge University Press: Cambridge, U.K.

Sherman, J., Davis, R., Owens, W., and Valdes, J. (2001). The autonomous underwater glider" spray". *Oceanic Engineering, IEEE Journal of*, 26(4):437–446.

Sheu, P. C.-Y. and Xue, Q. (1993). *Intelligent Robotic Planning Systems*, volume 3. World Scientific.

Simmonet, E., Dijkstra, H., and Ghil, M. (2009). *Bifurcation Analysis of Ocean, Atmosphere, and Climate Models. In 'Computational Methods for the Atmosphere and the Oceans'*, volume XIV, p. 187-229. Handbook of Numerical Analysis.

Soulignac, M., Taillibert, P., and Rueher, M. (2009). Time-minimal path planning in dynamic current fields. In *Robotics and Automation, 2009. ICRA '09. IEEE International Conference on*, pages 2473 –2479.

Stommel, H. (1989). The slocum mission. *Oceanography*, pages 22–25.

Tan, C. S., Sutton, R., and Chudley, J. (2004). An incremental stochastic motion planning technique for autonomous underwater vehicles.

Thompson, D. R., Chien, S. A., Chao, Y., Li, P., Arrott, M., Meisinger, M., Balasuriya, A. P., Petillo, S., and Schofield, O. (2009). Glider Mission Planning in a Dynamic Ocean Sensorweb. In *SPARK Workshop on Scheduling and Planning Applications, International Conference on Automated Planning and Scheduling*.

Thompson, D. R., Chien, S. A., Chao, Y., Li, P., Cahill, B., Levin, J., Schofield, O., Balasuriya, A. P., Petillo, S., Arrott, M., and Meisinger, M. (2010). Spatiotemporal path planning in strong, dynamic, uncertain currents. In *Proceedings of IEEE International Conference on Robotics and Automation*, pages 4778–4783.

Ueckermann, M. P. and Lermusiaux, P. F. J. (2011). 2.29 Finite Volume MATLAB Framework Documentation. Technical report, Massachusetts Institute of Technology, Cambridge, MA USA.

Ueckermann, M. P., Lermusiaux, P. F. J., and Sapsis, T. P. (2013). Numerical schemes for dynamically orthogonal equations of stochastic fluid and ocean flows. *Journal of Computational Physics*, 233:272–294.

Warren, C. W. (1990). A technique for autonomous underwater vehicle route planning. In *Autonomous Underwater Vehicle Technology, Proceedings of the Symposium on*, pages 201–205.

Webb, D. C., Simonetti, P. J., and Jones, C. P. (2001). Slocum: An underwater glider propelled by environmental energy. *IEEE Journal of Oceanic Engineering*, 26(4):447–452.

WHOI (2006). Shallow water experiment 2006. `http://acoustics.whoi.edu/sw06/`.

Wikipedia (2012). Underwater glider. `http://en.wikipedia.org/wiki/Underwater_glider`. [Online; accessed 18-Aug-2014].

Witt, J. and Dunbabin, M. (2008). Go with the flow: Optimal auv path planning in coastal environments. In *Proceedings of Australasian Conference on Robotics and Automation*.

Yang, K., Gan, S., and Sukkarieh, S. (2010). An efficient path planning and control algorithm for ruavs in unknown and cluttered environments. *Journal of Intelligent and Robotic Systems*, 57:101–122.

Zhang, W., Inanc, T., Ober-Blobaum, S., and Marsden, J. E. (2008). Optimal trajectory generation for a glider in time-varying 2D ocean flows B-spline model. In *Robotics and Automation, 2008. ICRA 2008. IEEE International Conference on*, pages 1083 –1088.